The Stability and Genesis of Rossby Vortices

GARETH P. WILLIAMS AND R. JOHN WILSON

Geophysical Fluid Dynamics Laboratory/NOAA, Princeton University, Princeton, New Jersey

(Manuscript received 30 December 1986, in final form 30 July 1987)

ABSTRACT

The stability and genesis of the vortices associated with long solitary divergent Rossby waves—the Rossby vortices—are studied numerically using the single-layer (SL) model with Jovian parameters. Vortex behavior depends on location and on balances among the translation, twisting, steepening, dispersion and advection processes. Advection is the main preserver of vortices. The solutions provide an explanation for the origin, uniqueness and longevity of the Great Red Spot (GRS).

In midlatitudes, stable anticyclones exist in a variety of sizes and balances: from the large planetary-geostrophic (PG) and medium intermediate-geostrophic (IG) vortices that propagate westward, to the small quasi-geostrophic (QG) vortices that migrate equatorward. These vortices all merge during encounters. Geostrophic vortices in the f_0-plane system adjust toward symmetry by rotating; those on the sphere adjust by rotating and propagating. Stable cyclones exist mainly at the QG scale or on the f_0-plane.

In low latitudes stable anticyclones exist only when a strong equatorial westerly jet and a significant easterly current are present to eliminate the highly dispersive equatorial modes. The permanence of a GRS-like, low-latitude vortex in a Jovian flow configuration is established by a 100-year simulation. At the equator, stable anticyclones exist only when they have the Hermite latitudinal form and the Korteweg-DeVries longitudinal form and amplitude range as prescribed by Boyd (1980). Soliton interactions occur between equatorial vortices of similar order.

Vortices can be generated at the equator by the collapse of low-latitude anticyclones. In mid or low latitudes, unstable easterly jets generate vortices whose final number depends mainly on the interaction history. Stochastically forced eddies cascade by wave interactions into zonal currents and by eddy mergers into a single Rossby vortex that thrives on the turbulence. Directly forced ageostrophic jets can make vortex drift more westerly and can change it from free state values of -10 m s^{-1} to forced state values of -5 m s^{-1} (as the GRS) or of $+5$ m s^{-1} (as the Large Ovals).

1. Introduction

Planetary motions are all predominantly geostrophic but they can take on different forms, depending on their scale relative to the Rossby deformation radius, L_R. Quasi-geostrophic (QG), intermediate-geostrophic (IG), and planetary-geostrophic (PG) motions occur at the small, medium, and large scales, respectively. These flow regimes are subsets of a general geostrophic system and can coexist if their scales are sufficiently separated (Williams, 1985a).

Rossby vortices occur in the single-layer (SL) system at the larger (IG, PG) planetary scales, both in midlatitudes and at the equator. Vortices in the two regions are related through their basis on the long solitary divergent Rossby wave, hence their name. Their different characteristics stem from their different forms of Rossby wave and nonlinearity (Boyd, 1980; Williams and Yamagata, 1984, hereafter WY84). Only anticyclones achieve a balance and a permanence and they merge during encounters in midlatitudes but behave like solitons at the equator.

The initial numerical study of Rossby vortices in WY84 was primarily concerned with examining their relevance to Jupiter's Great Red Spot (GRS) and Large Ovals. The solutions showed that vortices can exist in low latitudes for about 500 days in the absence of zonal currents and for about 5000 days in the presence of Jovian-style currents. They also showed that a single vortex can be generated by a weak shear instability and multiple vortices by a strong instability. Thus zonal currents appear to be essential to the stability and genesis of the GRS and the Large Ovals. But as a study of basic vortex properties, the WY84 research was compromised by three factors: 1) numerically, the computational diffusion was relatively strong and contributed to vortex decay; 2) physically, the vortices were simulated only in the highly dispersive low-latitude region; 3) diagnostically, there was no quantitative procedure for defining the dynamics.

Vortices can now, however, be defined accurately using the recently derived geostrophic potential-vorticity (GPV) equation. This equation describes the various processes acting on a vortex on a sphere: translation, twisting, steepening, dispersion and advection

Corresponding author address: Dr. Gareth P. Williams, Geophysical Fluid Dynamics Laboratory, Princeton University, P.O. Box 308, Princeton, NJ 08542.

(Williams, 1985a). In WY84 the importance of twisting was underestimated relative to the Korteweg-DeVries (KdV) elements (steepening and dispersion), even though its role in destroying low-latitude vortices was revealed by its elimination in a process model which allows gravity to vary as $\sin^2\theta$ to make the angular phase speed independent of latitude. In this paper, other process models, based on linearized height or momenta equations, allow selective examination of steepening and advection. The role of advection is most easily isolated in the f_0-plane system where it is the only process acting.

Our aim in this paper is to examine the stability, genesis, and interaction of Rossby vortices in all regions using a more accurate, less-dissipative SL prediction model and a more incisive, GPV diagnostic equation. In particular, we need to understand how stability depends on the size, strength, and spherical location of the vortex and on the existence of currents. We also need to know what factors control the number of vortices generated by shear instability or by stochastic forcing. For the GRS we would like to know when and how single vortex states arise and how vortex drift rates can be modified—the GRS mostly propagates westward, the Large Ovals mostly eastward. Because of this planetary interest we use "Jovian" parameters in the computations, but the results apply to any system with a small Rossby radius.

The connection between vortices in SL fluids and in continuously stratified atmospheres remains unclear despite attempts at isolating coherence regimes for baroclinic systems (Anderson and Killworth, 1979; Petviashvili and Yankov, 1982; Flierl, 1984; Romanova and Tseytlin, 1985). Although the SL model can be used to represent either barotropic or baroclinic modes in the ocean (Gill, 1982), its interpretation for Jupiter cannot be made precise in the absence of data about static-stability variations below the clouds. For now it is sufficient to regard the SL vortices as the simplest prototype of coherence relevant to the planet.

The study of geostrophic coherence began with the finding that solitary Rossby waves disperse in a barotropic model (Yeh, 1949) but that this dispersion is significantly slowed by linear divergence in the equivalent barotropic model (Bolin, 1956). Later it was found that this dispersion could be balanced completely by nonlinear momentum advection in the barotropic model to give the Rossby shear-soliton (Long, 1964), and by nonlinear divergence in the SL model to give the Rossby density-soliton (Clarke, 1971). The application of similar ideas to Jupiter began with the suggestion by Golitsyn (1970) that the GRS could be a free vortex because the planet has such a low dissipation rate. This proposal was explored for modons in QG barotropic and equivalent-barotropic models stabilized by zonal currents (Ingersoll, 1973; Ingersoll and Cuong, 1981), and for shear-solitons in QG baroclinic models (Maxworthy and Redekopp, 1976; Redekopp 1977). Circulation studies, however, suggested that QG scale modes are turbulent, not coherent, on Jupiter (Williams, 1979).

Analyses of the SL equations quickly resolved this impasse by showing that coherence occurs more naturally at the larger (IG, PG) scales and that it can coexist, by virtue of scale separation, with the turbulence occurring at the smaller (QG) scales (Petviashvili, 1980; Charney and Flierl, 1981; Yamagata, 1982; WY84). The large-scale SL coherence exists through the action of nonlinear divergence and produces vortices related to Clarke's (1971) density-soliton and Boyd's (1980) equatorial-soliton. Our numerical studies show these SL vortices to be stable and to be easily generated by shear instability or eddy forcing. Rossby vortices have also been produced in laboratory experiments (Antipov et al., 1981, 1986; Sagdeev et al., 1981). For a detailed discussion of the basic theory of planetary solitary waves, the review by Malanotte-Rizzoli (1982) is recommended.

We begin in §2 by describing the numerical SL model and in §3 by reviewing geostrophic wave and vortex theory for midlatitudes and the equator. The stability and interactions of Rossby vortices in current-free environments are examined for midlatitudes in §4 and for the equator in §6, with the midlatitude dynamics analyzed in detail using the GPV equation in §5. Section 7 describes the influence of stable zonal currents on low-latitude vortex behavior; §8, the genesis of vortices by unstable currents and by the mergers of stochastically forced eddies. A summary of this study is given in a review paper that describes the planetary observations and problems in greater detail (Williams, 1985b).

2. Numerical model

The basic equations for hydrostatically balanced motion in the shallow-water or single-layer (SL) system on a sphere can be written in the invariant form preferred for numerical representation:

$$u_t - (f+\zeta)v = -m^{-1}(gh + K)_x + D(u), \quad (1)$$

$$v_t + (f+\zeta)u = -(gh + K)_y + D(v), \quad (2)$$

$$h_t + m^{-1}(uh)_x + m^{-1}(mvh)_y = D(h), \quad (3)$$

where g represents either the full or reduced gravity; $\zeta = m^{-1}\{v_x - (mu)_y\}$, the vorticity; $K = \frac{1}{2}\mathbf{v}\cdot\mathbf{v}$, the kinetic energy; $f = 2\Omega\sin\theta$, the Coriolis term; $m = \cos\theta$, the sphericity; $(x, y) = a(\lambda, \theta)$ and (u, v), the longitudinal and latitudinal coordinates and velocities; and D, the small-scale diffusion operator.

A finite-difference representation suffices in solving (1)–(3) for vortices and also makes domain variation easy. To achieve the accuracy, stability and precision needed for very long, near-inviscid, divergent flow simulations, we use the formulation of Arakawa and Lamb (1981) which conserves potential enstrophy and

total energy. The velocities are defined on a staggered latitude–longitude grid centered on the height field and all variables are advanced using a leapfrog time-stepping and a weak Robert smoothing with a coefficient of 0.005. For calculating the GPV balances (see §3b and the Appendix), we switch to the simpler Sadourny (1975) formulation because it gives an exact geostrophic wind, whereas the complex Arakawa-Lamb scheme does not.

To control numerical instabilities, the small-scale enstrophy is removed by applying the biharmonic diffusion operator $D = \nu_4\nabla^4$ (where ν_4 is negative) to all three variables. The biharmonic operator only minimally dampens kinetic energy and essentially leaves the large scales inviscid. The diffusion coefficient used in most of our calculations implies decay times ($\tau_4 = L^4/4(2\pi)^4|\nu_4|$) of 1 day and 10^4 days for the gridscale and vortex scale, respectively. To avoid arbitrary adjustment the initial velocity $\mathbf{v}_0$ and height h_0 are chosen to be in geostrophic balance in midlatitudes and to be governed by Boyd's (1980) analytical solutions at the equator (see §3f).

We examine the vortices using parameter values believed to be appropriate to Jupiter's atmosphere (WY84), but the results apply to any system with a small Rossby radius. The primary SL scale, $L_R = (gH)^{1/2}/f$, depends upon the choice of g and H (the mean thickness). For Earth's atmosphere, the values $g = g_E/6$ and $H = H_E$ (or equivalently, $g = g_E$ and $H = H_E/6$) are often used and give $L_R = 1000$ km, where g_E and H_E are Earth's gravity and scale height. For Jupiter, similar relative values appear to be useful. Defining a normalized gravity $g^* = g/g_J$, most calculations are made with $g^* = 0.1$, $H = H_J = 10$ km, $a_J = 7.14 \times 10^4$ km, $\Omega_J = 1.763 \times 10^{-4}$ s^{-1}, $g_J = 26.4$ m s^{-2}, and $\nu_4 = -1 \times 10^4$ km^4 s^{-1}. Only deviations from this standard J set will be documented in figure captions.

The computational domains are atmospheric channels of sufficient width and breadth to isolate the main modes from the boundaries. Boundary conditions assume longitudinal periodicity and, on the lateral walls, no inflow and field symmetry (for the biharmonic diffusion). Higher resolutions are used for the smaller vortices and narrower jets, and for those flows subjected to a geostrophic potential-vorticity analysis (Table 1). Smaller values of ν_4 are used for the very small vortices.

TABLE 1. Resolution systems R1–R8 for longitude and latitude (in degrees) and for time (in minutes). Diffusion in 10^4 km^4 s^{-1}. Referred to by figure captions.

	$\Delta\lambda$	$\Delta\theta$	Δt	$-\nu_4$
R1	2.0	1.0	30	1.0
R2	2.0	0.5	15	1.0
R3	1.0	0.5	15	1.0
R4	0.75	0.75	15	1.0
R5	0.5	0.5	13	1.0
R6	0.5	0.4	10	1.0
R7	0.4	0.2	6	0.1
R8	0.15	0.1	3	0.01

3. Theory for Rossby vortices

We now briefly review the elementary linear and nonlinear theories that form the basis of our understanding of Rossby vortex dynamics. These ideas also guide the design and interpretation of the calculations in §4–8.

a. Linear modes

The natural linear oscillations of the SL system govern the propagation and dispersion character of Rossby vortices. Large-scale linear modes are best represented by the skewed functions of the general or equatorial β-planes. These eigenfunctions arise on introducing the general β-plane approximation $f = f_0 + \beta y$ into the SL Eqs. (1)–(3), linearizing and assuming wavelike disturbances of the form $\exp\{i(kx - \omega t)\}$ in longitude and time (Lindzen, 1967). This leads to the well-known Schroedinger equation for the latitudinal amplitude distribution $v(y)$:

$$v_{yy} - v\left[\frac{1}{gH}(f^2 - \omega^2) + k^2 + \frac{\beta k}{\omega}\right] = 0, \qquad (4)$$

and solutions in the form of parabolic cylinder functions. The classical midlatitude β-plane assumption, that f is constant except when it is differentiated, cannot be made for the large-scale motions and its trigonometric eigenfunctions apply only to the small (QG) scales.

The representation defined by (4) simplifies when the β-plane is centered at the equator and the eigenmodes become Hermite functions. The Rossby wave solutions for the equatorial β-plane then have the form $H_n(y^*)\exp(-0.5y^{*2})$ and the dispersion relation $\omega = -\beta k/\{k^2 + (2n + 1)(L_R)^{-2}\}$, when the ω^2 term in (4) is neglected, where H_n is the Hermite polynomial of order n and where $y^* = y/L_R$ defines the latitudinal scale in terms of the equatorial deformation radius, $L_R = (c_g/\beta)^{1/2}$, based on the reduced-gravity wavespeed $c_g = (gH)^{1/2}$. The long Rossby waves propagate at speeds $c = \omega/k = -c_g/(2n + 1)$ that increase rapidly as n decreases. When the β-plane is centered in midlatitudes the solutions tend toward the trigonometric or WKB form only for modes with a small lateral scale. Such Rossby waves have the form $\exp(ily)$ or $l^{-1/2}\exp(i\int l\,dy)$ and the dispersion relation $\omega = -\beta k/(k^2 + l^2 + L_R^{-2})$, where $L_R = c_g/f$ defines the midlatitudinal deformation radius. Their long waves propagate at speeds $c_\beta = -\beta L_R^2$ that increase toward the equator.

The equatorial β-plane modes have a wavelike latitudinal variation whose largest amplitude occurs in the last oscillation before exponential decay sets in at the turning points $y_t = a[(2n + 1)/\hat{e}]^{1/2}$, where $\hat{e} = (a/L_R)^2 = 2\Omega a/c_g$ is the Lamb parameter. Only as n be-

comes large do the eigenfunctions span all latitudes. Eigenfunctions with $(2n + 1) < (\pi/2)^2\hat{e}$, i.e., with $y_t < a\pi/2$, do not extend beyond the pole and so provide a valid representation of the lower-order Rossby waves (Lindzen, 1967). The midlatitude β-plane eigenfunctions then provide a reasonable representation of the higher-order modes. For Earth, the Lamb parameter is small ($\hat{e} = 3$), so the equatorial β-plane remains valid only for modes up to $n = 3$ and the midlatitude β-plane then provides a better representation of the predominantly QG-scale motions. For Jupiter, however, the Lamb parameter is large ($\hat{e} = 140$), so the equatorial β-plane remains valid up to $n = 150$ and the midlatitude β-plane then is accurate only for modes with a very small (<3°) latitudinal extent. This structural difference between the two planets was first noted by Golitsyn and Dikii (1966) and Lindzen (1967), and leads to a major problem in Jovian meteorology: what prevents the GRS, a large low-latitude disturbance, from generating the highly dispersive, low-order equatorial modes and thereby collapsing?

b. *The geostrophic potential-vorticity equation*

To describe large-scale nonlinear motions on a sphere we require the full SL equations. Fortunately, when geostrophy prevails, these equations can be reduced to a potential-vorticity equation that applies to all (PG, IG, QG) scales but involves only the height variable (Williams, 1985a). To obtain this geostrophic potential-vorticity (GPV) equation, (1) and (2) are inverted and the velocity is written as the sum of the geostrophic and ageostrophic components:

$$\mathbf{v}^g = \frac{g}{f}\mathbf{k} \times \nabla h, \quad \mathbf{v}^a = \frac{1}{f}\mathbf{k} \times \left\{\frac{D\mathbf{v}}{Dt} - D(\mathbf{v})\right\}, \quad (5)$$

where $\mathbf{k}$ is the vertical unit vector. Then the height equation (3) can be split into a geostrophic–ageostrophic form

$$h_t + h\nabla \cdot \mathbf{v}^g + \nabla \cdot (h\mathbf{v}^a) = D(h), \quad (6)$$

containing the five basic processes

$$h\nabla \cdot \mathbf{v}^g = \frac{g}{m} hh_x(f^{-1})_y, \quad (7)$$

$$\nabla \cdot (h\mathbf{v}^a) = \nabla \cdot \frac{h}{f}(\mathbf{k} \times \mathbf{v}_t) - \nabla \cdot \left(\frac{h}{f}\zeta\mathbf{v}\right) + \nabla \cdot \frac{h}{f}(\mathbf{k} \times \nabla K) - \nabla \cdot \frac{h}{f}(\mathbf{k} \times D(\mathbf{v})). \quad (8)$$

If we assume that geostrophy holds at O(1), then $\mathbf{v}$ may be approximated by $\mathbf{v}^g$ in (8) to reduce the exact Eq. (6) to an $O(\hat{\epsilon}^2)$ equation that involves only the height variable

$$h_t + \frac{g}{m} hh_x(f^{-1})_y - g\nabla \cdot \left(\frac{h}{f^2}\nabla h_t\right) - gJ\left(h, \frac{h\zeta}{f^2}\right) - J\left(\frac{h}{f}, K\right) - \nabla \cdot \frac{h}{f}(\mathbf{k} \times D(\mathbf{v}^g)) = D(h), \quad (9)$$

where $\zeta = g\nabla \cdot (f^{-1}\nabla h)$ and $K = g^2|\nabla h|^2/2f^2$ are now geostrophic quantities; $\hat{\epsilon}$ is the Rossby number and $J(h, \phi) \equiv m^{-1}(h_x\phi_y - h_y\phi_x)$ is the advection Jacobian for any scalar ϕ. The terms in (6)–(8) have the same identity as those in (9): the geostrophic divergence reduces to a translation and steepening, while the ageostrophic divergence splits into a dispersion, vorticity advection, kinetic-energy advection, and vorticity diffusion: all weighted by h.

To identify the different balances that occur at the different planetary scales, we nondimensionalize (9) by writing $h = H + \eta$ for the mean and deviation thicknesses, introducing the scales $(U, L, L/U, LUf_0/g, f_0)$ for the variables $(\mathbf{v}, y, t, \eta, f)$, and defining the Rossby, stratification and sphericity parameters: $\hat{\epsilon} = U/Lf_0$, $\hat{s} = (L_R/L)^2$, $\hat{\beta} = \beta L/f_0$. The GPV equation then has the nondimensional inviscid form

$$\eta_t - \hat{s}\nabla \cdot \left\{\frac{1}{f^2}\left(1 + \frac{\hat{\epsilon}}{\hat{s}}\eta\right)\nabla\eta_t\right\} - \frac{1}{m_0 f^2}\left(1 + \frac{\hat{\epsilon}}{\hat{s}}\eta\right)\eta_x - \frac{\hat{\epsilon}}{\hat{\beta}}\left(1 + \frac{\hat{\epsilon}}{\hat{s}}\eta\right)J\left(\eta, \frac{\zeta}{f^2}\right) - \frac{\hat{\epsilon}^2}{\hat{s}\hat{\beta}}J\left(\frac{\eta}{f}, K\right) = 0, \quad (10)$$

(i) (ii) (iii) (iv) (v)

which has three basic parameters and three major dynamical regimes (Charney and Flierl, 1982; Malanotte-Rizzoli, 1982; WY84; Williams, 1985a). At the QG scales ($\hat{s} \sim 1$), the terms (ii)–(v) drop out, so there is no steepening; at the PG scales ($\hat{s} \sim \hat{\epsilon}$), the terms (i) and (ii) drop out, so there is no dispersion; and at the IG scales ($\hat{s}^2 \sim \hat{\epsilon}$), the terms (ii), (iv), (v) drop out but all major processes remain. The GPV equation holds in mid- and low latitudes but it cannot describe phenomena—such as Boyd's (1980) solitons—that require the matching of contributions from both hemispheres.

In analyzing the numerical solutions, it is easier and more accurate to evaluate the exact implicit Eq. (6) than the approximate explicit Eq. (9); the latter is used only to interpret the former. To get a precise balance, the terms in (7) and (8) must be evaluated from their finite-difference counterparts in the prediction code. As noted in §2, using the Sadourny (1975) scheme simplifies both the extraction of accurate $\mathbf{v}^g$ and $\mathbf{v}^a$ values and the definition of the divergence components; see the Appendix for details.

c. *Nonlinear response in midlatitudes*

To simplify our discussion of vortex theory, we retain only the most important terms of (10), set their coef-

ficients to unity, and create the representative β-plane equation:

$$\eta_t - \eta_x - \eta\eta_x - \nabla\cdot(1+\eta)\nabla\eta_t + 2y\eta_x - J(\eta, \nabla^2\eta) = 0. \quad (11)$$

The nonlinear dispersion term $\nabla\eta\cdot\nabla\eta_t$ is found to be significant in the numerical solutions even though it does not appear in the formal analysis. Equation (11) forms a modified IG equation and describes very strong vortices at the intermediate scale. The first two terms dominate and describe Rossby long-wave propagation, where $c_\beta = -1$ nondimensionally. The twisting term $2y\eta_x$ comes from the latitudinal variation in c_β caused by the f^{-2} factor: c_β varies from -1.5 m s^{-1} at $\theta = 45°$ to -8.4 m s^{-1} at $\theta = 20°$ for the Jovian parameters.

Although twisting prevents simple KdV balances, the KdV terms in (11) do control the size, strength, shape and speed of many vortices. To be more precise, the first four terms in (11) control such features and they constitute a regularized long-wave (RLW) equation (Benjamin et al., 1972), modified by a nonlinear dispersion term, rather than a pure KdV equation. The difference is significant when the vortices are strong. For convenience we refer to the first four terms of (11) as the Rossby-RLW equation.

The simple one-dimensional RLW equation

$$\eta_t - \eta_x - \eta\eta_x - \eta_{xxt} = 0, \quad (12)$$

reduces to the KdV differential equation

$$(1+c_1)\eta_{xx} = c_1\eta - \frac{1}{2}\eta^2, \quad (13)$$

on writing $\eta_t = (1+c_1)\eta_x$, and so has solitary wave solutions of the form

$$\eta = 3c_1\,\mathrm{sech}^2\left\{\frac{c_1^{1/2}}{2(1+c_1)^{1/2}}(x + (1+c_1)t)\right\}, \quad (14)$$

where c_1 is the westward phase speed gain due to the finite amplitude and nonlinearity. The full Rossby-RLW equation reduces to what we call the Rossby-KdV equation:

$$[(1+c_1)(1+\eta)]\left[\frac{1}{r}(r\eta_r)_r\right] = c_1\eta - \frac{1}{2}\eta^2 - \frac{(1+c_1)(\eta_r)^2}{2}, \quad (15)$$

if the nonintegrable term $\int \eta_x\nabla^2\eta dx$ is small. Compared to the standard radial-KdV equation (Flierl, 1979), (15) has extra factors $(1+c_1)(1+\eta)$ on the left side and an extra term $(\eta_r)^2$ on the right side. The equation shows that steepening and dispersion balance radially even though changes are forced by a unidirectional propagation.

The Rossby-KdV and radial-KdV eigenfunctions in Fig. 1, obtained by solving (15), with and without the extra terms, as an eigenvalue problem for c_1, have quasi-Gaussian forms and differ more strongly from each other as the amplitude increases. The Rossby-KdV soliton is almost twice as wide and fast as the radial-KdV soliton when the amplitude equals 10 km. Most of the gain comes from the nonlinear dispersion factors $(1+c_1)(1+\eta)$: the large amplitude makes $c_1 \sim 1$ even though η decreases away from the vortex center. The nonintegrable term makes a negligible contribution to these solutions.

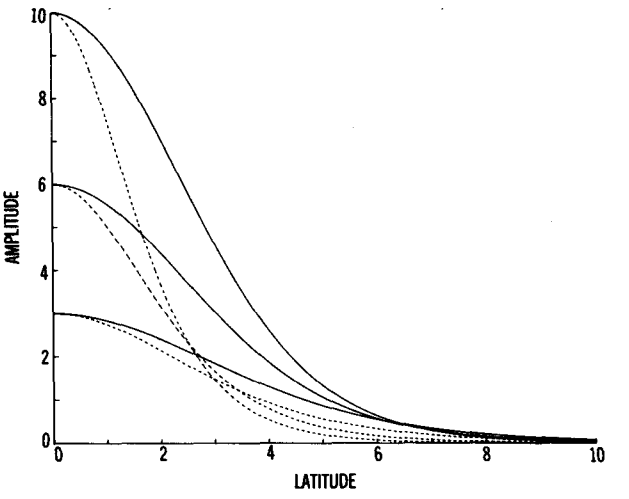

FIG. 1. Eigenfunctions of the radial-KdV (dashed lines) and Rossby-KdV (solid lines) equations, for vortices with amplitudes of 3, 6, 10 km. Corresponding eigenvalues (nondimensional c_1) are (0.192, 0.389, 0.657) and (0.284, 0.577, 0.974).

If vortices are initialized using solutions to (15) in SL models from which twisting has been removed (see §3d), their adjustment is minimal and confirms that the Rossby-KdV terms control the speed, size and shape. Generally, however, the twisting cannot be ignored and in the linear version of (11)

$$(c_1\eta + 2y\eta - \eta_{yy})_x = 0; \quad (16)$$

it leads to Airy eigenfunctions and the equatorward propagation of long waves. Such asymmetric meridional dispersion breaks a local KdV balance and activates the advection Jacobian, which may or may not reestablish equilibrium.

We can get some idea of how the various processes react to a simple asymmetry by considering the ellipse

$$\eta = \eta_0 \exp\left\{-\frac{1}{2}\left(\frac{x^2}{x_1^2} + \frac{y^2}{y_1^2}\right)\right\}.$$

For such a storm, the propagation (P), dispersion (D), steepening (S), twisting (T) and Jacobian (J) of (11) may be evaluated as

$$P = -\frac{x\eta}{x_1^2}, \quad D = +\frac{x\eta}{x_1^2}\left[\frac{3}{x_1^2} + \frac{1}{y_1^2} - \frac{x^2}{x_1^4} - \frac{y^2}{y_1^4}\right], \quad (17)$$

and

$$S = -\frac{x\eta^2}{x_1^2}, \quad T = +\frac{2xy\eta}{x_1^2}, \quad J = -\frac{2xy\eta^2}{x_1^4 y_1^4}(x_1^2 - y_1^2). \tag{18}$$

The P, S, D terms are bipolar (about $x = 0$) and could adjust the amplitude into a KdV-like balance. The T, J terms, however, are quadrapolar (about $x = 0, y = 0$) and disrupt such a balance. The T term acts to stretch the vortex along a southwest–northeast axis, while J counters it in all four quadrants to restore radial symmetry. The J, S terms can balance the T, D terms only for anticyclones ($\eta_0 > 0$) as the latter pair switch sign for cyclones. Only the Jacobian is sensitive to the shape of the vortex and can easily change sign and form. On the f_0-plane, the Jacobian is the only geostrophic process acting and restores symmetry ($x_1 = y_1$) by rotating anticyclones clockwise and cyclones anticlockwise (see §4).

d. *Process models*

We can illustrate the action of the various terms by solving special forms of the SL model. The twisting, steepening, and advection can be eliminated either singly or together by mathematical devices.

The first process model, illustrated in Fig. 2a, removes the twisting from the SL model by varying the gravity (or H) as $\sin^2\theta$ to cancel f^2 variations and make the angular velocity $c_\beta/(a\cos\theta)$ independent of latitude. On the β-plane this is equivalent to setting $g = g_0(1 + Gy)$ so that (11) becomes

$$\eta_t - \eta_x - (1 + G)\eta\eta_x - \nabla\cdot(1 + \eta)\nabla\eta_t + 2y\left(1 - \frac{G}{2}\right)\eta_x - J(\eta, \nabla^2\eta) = 0, \tag{19}$$

with the steepening tripling and twisting vanishing for $G = 2$. The initial vortex is given by the geostrophic Gaussian state

$$h_0 - H = H_0 \exp\left[-\frac{1}{2}\left\{\left[\frac{\theta - \theta_0}{\delta\theta}\right]^2 + \left[\frac{\lambda - \lambda_0}{\delta\lambda}\right]^2\right\}\right], \tag{20}$$

$$u_0 = \frac{-g}{f}h_{0y}, \quad v_0 = \frac{g}{mf}h_{0x}, \tag{21}$$

where H_0 is the vortex amplitude; $(\delta\lambda, \delta\theta)$ the half widths; and (λ_0, θ_0) the center. The P1 solution confirms that, in the absence of twisting, vortices have the form predicted by the Rossby-KdV Eq. (15) and are stable and long lived. The vorticity and kinetic-energy Jacobians vanish because the radial shape is maintained but they reenter during collisions and produce mergers, not KdV-like soliton encounters, unless they too are mathematically removed, as in the next example.

The second process model, illustrated in Fig. 2b, eliminates the advection Jacobians from the SL model by linearizing the momentum equations, omitting ζ from the Coriolis terms and K from the pressure gradients in (1)–(3). The twisting then distorts the large vortex along the southwest–northeast axis without constraint. The vortex cannot achieve a local KdV-like balance and migrates equatorward, steepening and shrinking to reduce the twisting and retain its strength. The corresponding vortex in the full SL model is shown in Fig. 4. Clearly, an anticyclone subjected to twisting cannot exist without the advection Jacobians.

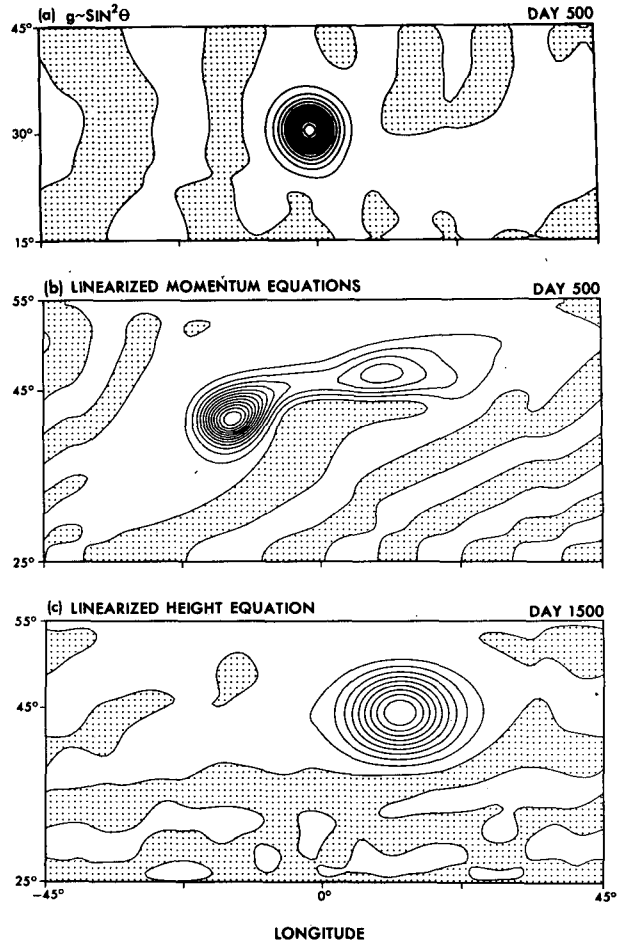

FIG. 2. Process solutions P1–P3: Vortices in special models. Height η has shaded negatives. Resolution: R3. Initial state: geostrophic Gaussian vortex as (20), (21). Cases: (a) P1, no twisting, CI = 0.25 km, H_0 = 3 km, $\delta\lambda = 3.5°$, $\delta\theta = 3°$, $\lambda_0 = 0°$, $\theta_0 = 30°$; $g^* = 0.1\ \sin^2\theta/\sin^2\theta_0$. Properties at 30°: $c = -4.4$ m s^{-1}, $c_\beta = -3.6$ m s^{-1}, L_R = 920 km. (b) P2, no advection, CI = 1 km, initially as (c). (c) P3, no steepening, CI = 1 km, H_0 = 10 km, $\delta\lambda = 6°$, $\delta\theta = 3°$, $\lambda_0 = 0°$, $\theta_0 = 45°$.

The third process model, illustrated in Fig. 2c, linearizes the SL height Eq. (3) to the form

$$h_t + H\nabla\cdot\mathbf{v} = D(h) \tag{22}$$

to eliminate the steepening. This device also simplifies the other geostrophic processes in (9), but they retain their essential character. Although the vortex no longer has a KdV component, it survives easily. Evaluating the various GPV terms shows them to be small and to have the elliptic-vortex forms of (17) and (18), with the Jacobian balancing the dispersion and twisting (Table 3). This anticyclone behaves almost like a propagating f_0-plane vortex, in that all processes tend towards zero and the vortex can have any size. (The f_0-plane process model is discussed in §4c).

The fourth process model uses a low-amplitude (linear) vortex to illustrate the character of long-wave dispersion (Fig. 3). We place the vortex in low latitudes where the dispersion is more rapid and harder to control, but a similar dispersion occurs in midlatitudes. In the P4 solution, weak low-latitude vortices disperse equatorward because of the latitudinal variation in the long-wave phase speed (twisting), in keeping with (16). The vortex creates a wave train that propagates at a rate given by the meridional group velocity (cf. Killworth, 1979). The cross-equatorial flow is more clearly seen in the u field because the geostrophic height disturbances are small near the equator. The theoretical solution to the linearized equatorial β-plane equations, obtained by decomposing the initial vortex into a Fourier-Hermite set of Rossby modes and multiplying each coefficient by its respective $\exp[-i\omega_n(k)t]$ (see Boyd, 1983), matches this solution and confirms the geostrophic character of the linear dynamics.

These four process solutions suggest that Rossby vortices lie between the two dynamical extremes represented by the Rossby-KdV solitons and the f_0-plane vortices. Steepening and dispersion dominate the first, advection controls the second, and twisting prevents both from being realized simply. Equatorial anticyclones also remain stable in the linearized v_t or h_t models, provided that the corresponding advection or steepening contributions to Boyd's coefficients in (27) are omitted when defining the initial state. Such omissions alter the vortex size. Low-latitude vortices are subject to a strong asymmetric dispersion and stabilizing them poses a major problem, one relevant to the GRS.

e. Process summary

Stable vortices can exist on a sphere in a variety of balances because the nonuniform propagation activates the various processes in ways that depend on the vortex scale. How the processes act may be summarized as follows:

1) LINEAR TWISTING

When anticyclones are large, the linear twisting $(c_\beta - c_\beta{}^0)\eta_{x'}$ is large and provides the main destabilizing process. The twisting destabilizes by dispersing long waves in the equatorward direction and thereby stretching vortices along the southwest–northeast axis. The tilt decreases as the vortex disperses. Twisting is stronger in low latitudes but is absent from equatorial vortices because each is based on a single meridional mode. Twisting is revealed by the initial adjustment of low-amplitude vortices, and by its absence in f_0-plane

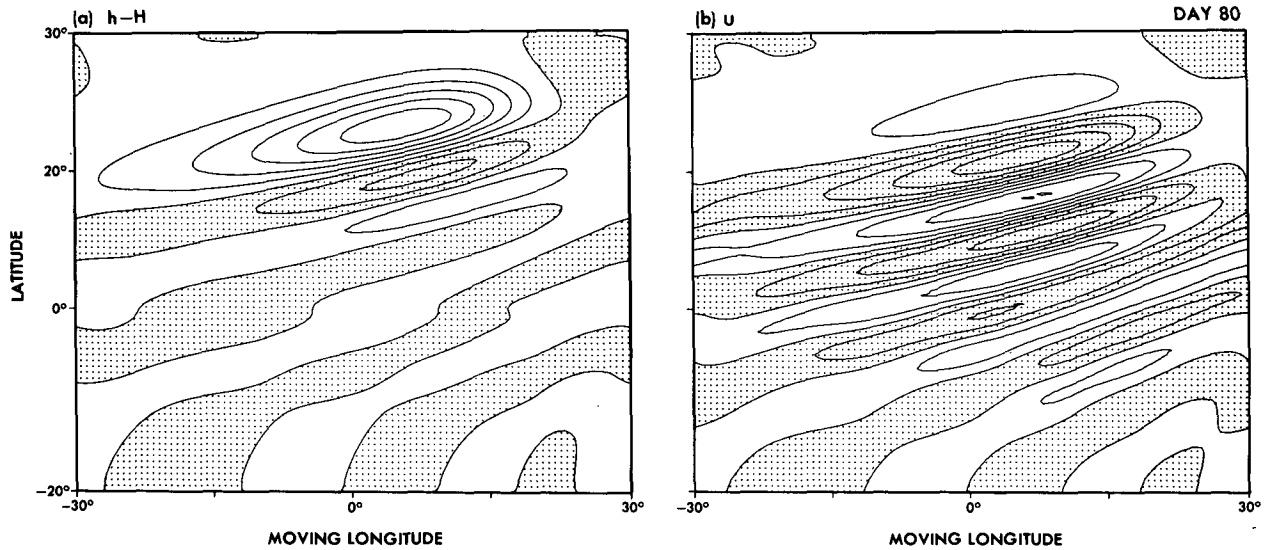

FIG. 3. Process solution P4: Meridional dispersion of a weak anticyclone in low latitudes. (a) Height η with CI = 10 cm, (b) u with CI = 0.1 cm s^{-1}; with axes moving at $c_a = c_\beta(20°) = -8.4$ m s^{-1}. Resolution: R1. Initial state: geostrophic Gaussian vortex with $H_0 = 5$ m, $\delta\lambda = 6°$, $\delta\theta = 3°$, $\lambda_0 = 0°$, $\theta_0 = 20°$.

or $g(\sin^2\theta)$ cases. It can also be eliminated by special zonal currents—see §7c.

2) STEEPENING AND NONLINEAR TWISTING

When anticyclones are large and strong, the steepening $c_\beta(y)\eta\eta_x$ has a nonlinear twisting factor that enhances vortex asymmetries. When unchecked, steepening breaks anticyclones on the western edge, cyclones on the eastern. Stable vortices can exist without it. Steepening is revealed by its dominance in strong or $g(\sin^2\theta)$ vortices, and by its absence in linearized-h_t or f_0-plane cases.

3) DISPERSION

Short-wave dispersion is the main destroyer of small and midsize vortices, but it can be checked by advection or steepening if the vortex is strong. The dispersion of energy is revealed by the waves radiating from small low-amplitude vortices and by its absence on the f_0-plane. Short waves propagate toward the west, pole, and equator.

4) ADVECTION

Vorticity advection $J(h, h\zeta/f^2)$ is the main preserver of vortices. It possesses a great flexibility, an ability to adjust in form and sign about the limiting radial state to restore symmetry and counter imbalances forced by other processes, but it rarely forces the balance. Its flexibility allows a variety of balances: in large vortices, it matches steepening; in small, dispersion; and in medium, it combines with steepening to match dispersion and twisting. Kinetic-energy advection becomes significant only in very small, strong vortices or in low latitudes. Symmetrization is revealed by the f_0-plane and $g(\sin^2\theta)$ adjustments and by its absence in the linearized-$\mathbf{v}_t$ model.

f. Nonlinear response at the equator

At the equator, stable vortices are limited to the narrow class of anticyclones described by Boyd (1980). The vorticity advection, rather than the height steepening, produces most of the equatorial KdV-concentration term through the self interaction of components lying on both sides of the equator. The GPV equation lacks a simple connection with Boyd's KdV equation because it cannot describe processes that act across the equator.

To see which processes are involved in the equatorial vortices, we summarize Boyd's analysis and evaluate the terms contributing to his KdV equation. For equatorial disturbances measured relative to a reference frame moving at the linear long-wave speed c, the zero-order equations on the equatorial β-plane can be solved in terms of Hermite polynomials of order n and the first-order v^1 equation can be written as

$$v^1_{yy} - \left(\frac{1}{c} + y^2\right)v^1 = Q_1 + Q_2 + Q_3, \tag{23}$$

where the functions of the zero-order terms are given by

$$Q_1 \equiv -\left(y + \frac{1}{c}\frac{\partial}{\partial y}\right)(u^0_t + u^0u^0_x + v^0u^0_y), \tag{24}$$

$$Q_2 \equiv +(c^2 - 1)v^0_{xx}, \tag{25}$$

$$Q_3 \equiv -\left(\frac{y}{c} + \frac{\partial}{\partial y}\right)[\eta^0_t + (u^0\eta^0)_x + (v^0\eta^0)_y], \tag{26}$$

and where quantities are nondimensioned with respect to c_g, L_R and H. The $Q_{1,2,3}$ terms originate in the u, v, η equations, respectively. On substituting the zero-order solution into these expressions and applying the orthogonality condition to eliminate the secular term, the Q terms regroup into tendency, concentration and dispersion terms to give a KdV equation for $v(x, t)$:

$$Av_t - Bvv_x - Cv_{xxx} = 0. \tag{27}$$

The positive coefficients A, B, C depend on integrals of the terms in (24)–(26) weighted by the Hermite functions.

To identify which terms in (24)–(26) make the most important contribution to the KdV dynamics, we compute the various integrals forming the coefficients of (27) for the $n = 1, 3, \cdots, 15$ modes. All KdV concentration terms originate in the advection of u^0 and η^0; all KdV tendencies, in the u^0 and η^0 tendencies; and all dispersion, with v^0. The results in Table 2 show that the u^0 advection (items 7 and 8) dominates and contributes at least twice as much as the η^0 steepening to the concentration term. Some of the terms active in midlatitude vortices do nothing here and the others are grouped differently. On forming the sum of the terms, defining $\alpha_n = B/A$ and $\gamma_n = C/A$, and allowing for Hermite-function normalization (which keeps α_n near unity), we find that the coefficients in Table 2 agree with Boyd's (1980, 1983) values.

Solutions to (27) have the classical form:

$$v(x, y, t) = V \exp\frac{(-y^2)}{2} H_n \operatorname{sech}^2\left[\left(\frac{\alpha_n}{\gamma_n}\frac{V}{12}\right)^{1/2} \times \left(x - ct + \frac{\alpha_n V t}{3}\right)\right], \tag{28}$$

in the stationary reference frame, where the amplitude V increases the easterly phase velocity by $\alpha_n V/3$ and produces an effective wavenumber

$$k_n = \left(\frac{\alpha_n}{\gamma_n}\frac{V}{12}\right)^{1/2}.$$

This solution is used to create the initial states for the computations in §6. The $n = 1$ solution is stable for a wide range of amplitudes but other modes become un-

TABLE 2. Contributions to the coefficients of Boyd's KdV equation for equatorial solitons from the zero-order terms of Eqs. (24)–(26) multiplied by Hermite functions and integrated over y. Superscripts have been omitted.

		n							
	Coefficient	1	3	5	7	9	11	13	15
1	$-yu_t$	0	0	0	0	0	0	0	0
2	$-c^{-1}u_{ty}$	4.5	24.5	60.5	112.5	180.5	264.5	364.5	480.5
3	$-c^{-1}y\eta_t$	4.5	24.5	60.5	112.5	180.5	264.5	364.5	480.5
4	$-\eta_{ty}$	0	0	0	0	0	0	0	0
	$\sum_1^4 = A$	9.0	49.0	121.0	225.0	361.0	529.0	729.0	961.0
5	yuu_x	0.2981	0.5012	0.6191	0.7108	0.7881	0.8558	0.9167	0.9722
6	yvu_y	0.7950	1.0576	1.2699	1.4439	1.5934	1.7256	1.8452	1.9547
7	$c^{-1}(uu_x)_y$	3.7403	7.2978	11.347	15.549	19.846	24.215	28.644	33.126
8	$c^{-1}(vu_y)_y$	0.8673	7.5168	4.3570	6.2960	8.3021	10.359	12.457	14.596
9	$c^{-1}y(u\eta)_x$	0.1626	1.8856	3.6592	5.5283	7.4693	9.4663	11.509	13.592
10	$c^{-1}y(v\eta)_y$	1.0842	2.0751	3.1465	4.2427	5.3555	6.4817	7.619	8.769
11	$(u\eta)_{xy}$	1.4094	1.2618	1.3955	1.5353	1.6654	1.7853	1.8960	1.9990
12	$(v\eta)_{yy}$	−1.0088	−1.1513	−1.3320	−1.4908	−1.6312	−1.7575	−1.8730	−1.9790
	$\alpha_n = (\sum_5^{12} = B)/A$	0.8161	0.3152	0.2022	0.1503	0.1202	0.1004	0.0864	0.0760
13	$-(c^2 - 1)v_{xx}$	0.8889	0.9796	0.9917	0.9955	0.9972	0.9981	0.9986	0.9990
	γ_n = (term 13 = C)/A	0.09876	0.01999	0.00819	0.00442	0.00276	0.00189	0.00137	0.00104

stable if V is not kept small. We select $V \approx 0.1$ for $n = 1$ to keep velocities below $c_g/2$, and $V \approx 0.01$ for $n \geq 3$ to maintain stability. The easterly phase speed of equatorial vortices is based on the dimensional Rossby long-wave speed $-c_g/(2n + 1)$, which equals -55 m s^{-1} and -25 m s^{-1} for $n = 1$ and 3. The magnitude of V also controls the longitudinal scale, with stronger vortices being shorter. In our calculations, the equatorial vortices have 22° to 45° longitudinal scales.

The Boyd-type of vortex can also exist near the equatorward wall of a midlatitude β-plane and be described in terms of parabolic cylinder functions, Clarke (1971). Zonal flows may provide such a boundary (cf. Fig. 19).

4. Vortices in midlatitudes (no zonal flow)

In this section, we present solutions to the SL Eqs. (1)–(3) that illustrate the main properties of Rossby vortices in midlatitudes: their stability, shape selection, and merging. The figures shade negative values and occasionally use reference frames that move westward at speeds close to the Rossby long-wave speed. Their captions give the computational details.

a. Long-lived anticyclone at $\theta_0 = 45°$

Our calculations show that midlatitude anticyclones are long-lived if they are strong and substantially larger than the deformation radius, in agreement with the analyses of Charney and Flierl (1981) and Malanotte-Rizzoli (1982). The first midlatitude solution, M1 in Fig. 4, illustrates this stability. As it propagates, the vortex adjusts its size and shape towards the quasi-Gaussian form of the Rossby-KdV balance, while keeping the amplitude constant at 10 km. The M1 vortex would only need to adjust latitudinally if it had a more-circular initial form, with $\delta\lambda = 4.2°$ and $\delta\theta = 3°$ at $\theta_0 = 45°$. Twisting and advection, however, concentrate the poleside flow and force deviations from a KdV form. Weak Rossby waves are generated by the vortex and propagate to the south and west.

The vortex travels steadily westward at a speed $c(45°) = -1.9$ m s^{-1} that exceeds the longwave speed $c_\beta(45°) = -1.5$ m s^{-1} by an amount consistent with the Rossby-KdV solution. (A large vortex has different propagation velocities at different latitudes; only the central value is given.) This westward drift produces an upflow in the western half and a downflow in the eastern half. The (v, u, w) velocities reach peaks of (15, 20, 0.001) m s^{-1}. The M1 vortex, chosen to compare with the GRS in size, has a diameter of 17 000 km and thus qualifies as a very large vortex relative to the Rossby radius ($L_R = 640$ km). If we assume the vortex has a length scale L equal to the diameter divided by π and a velocity scale $U = 10$ m s^{-1}, then the values of the nondimensional parameters $\hat{\beta} = 0.05$, $\hat{\epsilon} = 0.01$, $\hat{s} = 0.02$ imply via the crude ordering relation $\hat{s} \sim \hat{\beta}$, $\hat{\epsilon} \sim \hat{\beta}$ that the storm lies more in a PG_2 than an IG dynamical regime (WY84, Table 1). The GPV analysis in §5 supports this conclusion to some extent.

Additional calculations show that M1-size vortices whose amplitudes lie below 5 km disperse at amplitude-

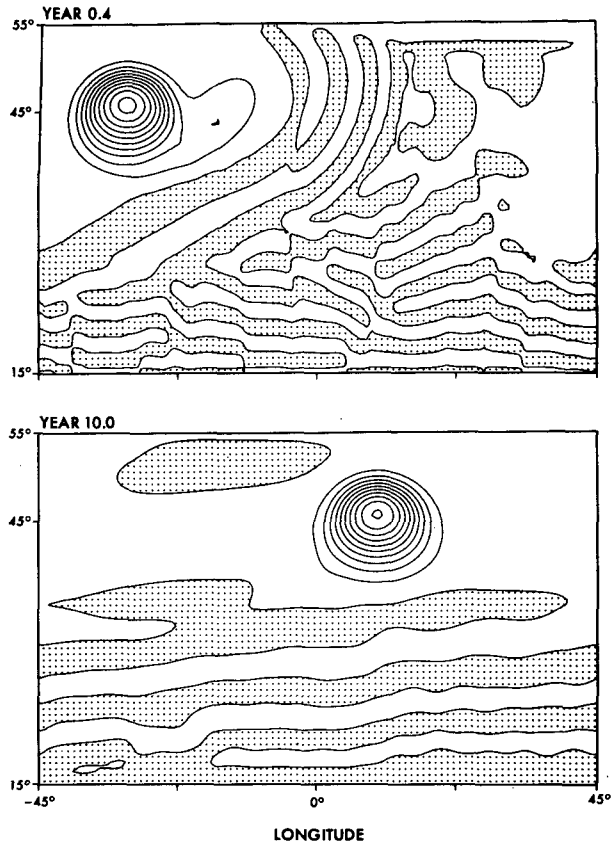

FIG. 4. Midlatitude solution M1: Longevity of anticyclones. Height η has contour interval CI = 1 km, and axes scaled to lengths at 45°. Resolution: R3. Initial state: geostrophic Gaussian vortex with H_0 = 10 km, $\delta\lambda = 6°$, $\delta\theta = 3°$, $\lambda_0 = 0°$, $\theta_0 = 45°$. Properties: $c = -1.9$ m s^{-1}, $c_\beta(45°) = -1.5$ m s^{-1}, $L_R(45°) = 640$ km.

dependent rates. Calculations for M1-size vortices at other latitudes show that when $\theta_0 = 30°$ decay is very slow, but when $\theta_0 = 20°$ decay occurs even for large amplitudes, being only slightly slower for $H_0 = 20$ km than for $H_0 = 10$ km. Smaller stable vortices can exist at $\theta_0 = 45°$ and are presented in §5.

b. *Cyclone collapse at $\theta_0 = 45°$*

The M2 solution in Fig. 5 shows the behavior of a cyclone having an initial amplitude of −4 km and the same size and shape as the M1 anticyclone. To keep the flow centered, changes are shown in a reference frame moving westward at $c_a = c_\beta(45°) = -1.5$ m s^{-1}. Cyclones, while they last, propagate at c_β but anticyclones move at faster amplitude-dependent rates.

The M2 cyclone evolves by first steepening on its eastern side. [Unequilibrated anticyclones steepen to the west (Fig. 9).] The steepening produces short Rossby waves which, because of dispersion, lag behind the main vortex. The strongest of these forms an anticyclone around which the cyclone curves because of its slower drift rate. More solitary waves grow at the interface and the cyclone eventually collapses completely into four stable anticyclones.

The cyclone distorts and collapses rapidly because the steepening and advection are the same sign as the dispersion and twisting and so enhance the decay. Thus, stronger cyclones collapse more rapidly than weaker ones. The difference in stability between cyclones and anticyclones reveals that these vortices are subject to IG or PG, not QG, dynamics. All four major processes act on the cyclone: twisting elongates it, advection rotates it, steepening in the east breaks it into anticyclones and generates waves that lag because of dispersion.

c. *Vortex adjustment on the f_0-plane*

To understand how the various processes act in adjusting an anticyclone towards symmetry and equilibrium, it helps to consider the simpler f_0-plane system first. Advection[1] is the only process acting on geostrophically balanced f_0-plane vortices and it tends to reduce itself by symmetrizing the flow. The F1 solution in Fig. 6 shows how an elongated Gaussian anticyclone with a 3:1 axis ratio attains the long-lived symmetrical state by rotating clockwise (cyclones rotate anticlockwise) and shedding two minor anticyclones. In the first phase (days 0–1000), the vortex rotates through 90°, sheds the two minors and reduces its asymmetry. The vortex continues to rotate until interactions with the two minors, beginning at days 1800 and 4800, have made it circular.

The shedding of minors by elliptical vortices contrasts with the shedding of thin filaments by inviscid two-dimensional, constant-vorticity ellipses in contour dynamics (Dritschel, 1986). It can, however, be explained as an eccentricity-dependent instability (Cushman-Roisin, 1986). According to (18), the shedding occurs because the Jacobian rotates the ellipse differentially. Our other calculations show that when f_0 is weaker, the vortices rotate and adjust more rapidly, and that when vortices are more elongated, with a 6:1 axis ratio, they still produce only two minors.

d. *Vortex interaction on the f_0-plane*

Although f_0-plane encounters must be forced by placing the nonpropagating vortices in overlapping configurations, they do provide the simplest example of the merging process. In Fig. 7 two identical circular anticyclones initially have centers 16° apart and a moderate overlap up to the 2 km contour. As the pair rotate clockwise, at a rate comparable to that of the elongated F1 vortex, their cores merge continuously to the 7 km level. After completing the merger, the vortex behaves like the F1 case and sheds two minors at 90° to the original axis. The merging corresponds to the

[1] Vorticity advection is normally the dominant advection; kinetic-energy advection is weak, except in extreme cases.

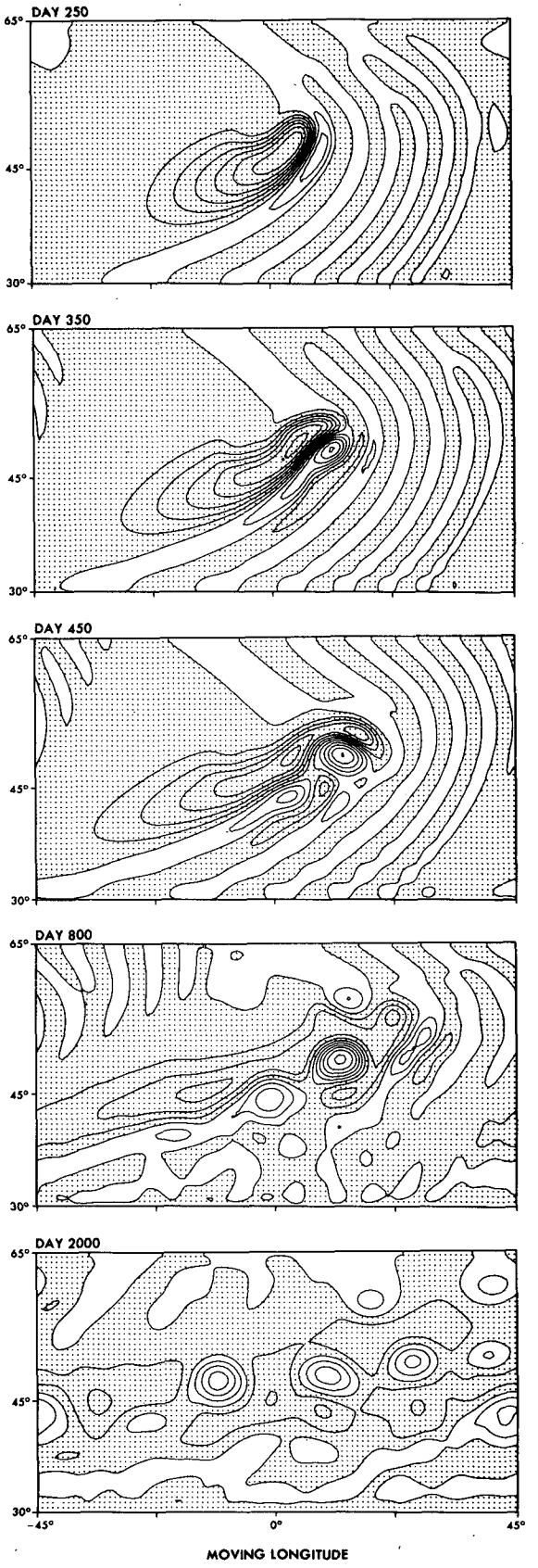

upscale energy decascade in two-dimensional turbulence, while the shedding corresponds to the downscale entrophy cascade. In the absence of a KdV coupling between size and strength, the merger produces a vortex of larger size rather than one of larger amplitude.

e. *Vortex adjustment on the sphere*

Vortex adjustment on the sphere, unlike on the f_0-plane, depends on the orientation of the asymmetry. Figures 8 and 9 illustrate the adjustment of latitudinally and longitudinally elongated anticyclones. In both configurations, the initial tendency of asymmetric anticyclones to rotate clockwise occurs but is modified in different ways by the westward propagation.

As the latitudinally elongated vortex rotates, it sheds two minors just as the f_0-plane case (Fig. 8). The three vortices then separate in longitude because phase speeds increase for lower latitudes and for higher amplitudes. These two factors almost compensate for the main vortex and the southern minor which move away from the northern minor at almost the same rate (the speed of the reference frame). The vortices do not interact because they propagate at well-separated latitudes.

As the longitudinally elongated anticyclone begins to propagate westward and to rotate clockwise, its core moves into the western half and steepens (Fig. 9). The western minor cannot break off and is absorbed by the speedier core vortex. Two eastern minors form in the long tail but only one breaks off. The adjusted configuration consists of the main vortex, one eastern minor and secondary blobs. The main vortex eventually laps and reabsorbs the other elements.

The adjustments in Figs. 8 and 9 both result in a smaller, more symmetric vortex whose final size, strength and shape resemble that of the M1 vortex. The vortices adjust their shape and size according to the Rossby-KdV balance while keeping their amplitude constant. This differs from the f_0-plane case in Fig. 6 where adjustment is toward a size determined mainly by the initial state. The adjustment in Fig. 9 corresponds to the classical KdV breakdown of a large disturbance into one or more solitons, arranged in amplitude order, plus a dispersive tail. However, the twisting and the Jacobian prevent a full realization of a simple KdV dynamics.

f. *Vortex interaction at $\theta_0 = 45°$*

Stronger vortices move more rapidly westward than do weaker vortices and so interactions in which vortices merge, partially or fully, occur readily. Figure 10 illustrates the interaction between two anticyclones, ini-

FIG. 5. Midlatitude solution M2: Collapse of a cyclone. Height η has CI = 0.5 km and axes moving at $c_a = c_\beta(45°) = -1.5$ m s^{-1}. Resolution: R3. Initial state: geostrophic Gaussian vortex with $H_0 = -4$ km, $\delta\lambda = 6°$, $\delta\theta = 3°$, $\lambda_0 = 0°$, $\theta_0 = 45°$.

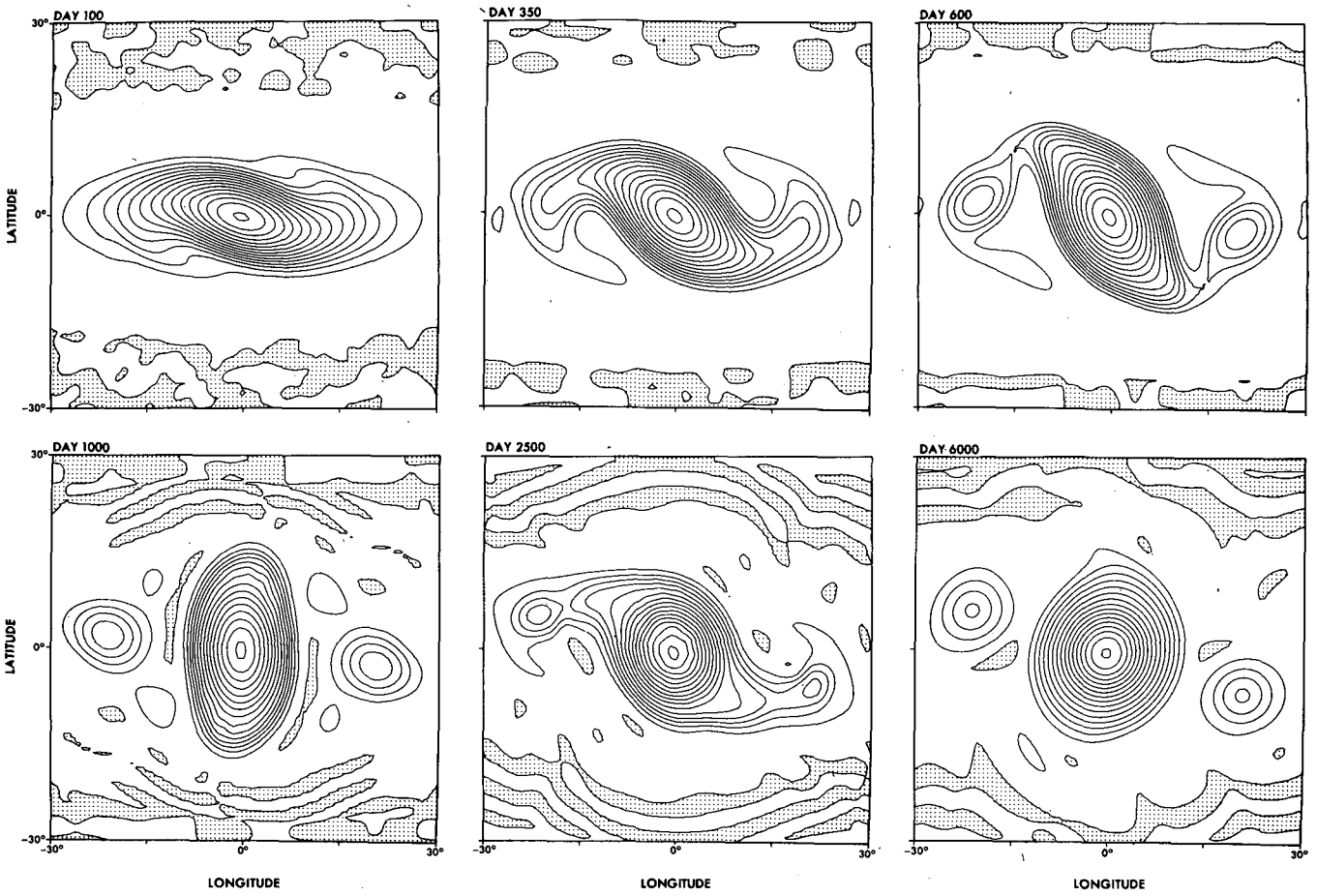

FIG. 6. The f_0-plane solution F1: Adjustment and longevity of anticyclones. Height η has CI = 1 km and axes relative to an arbitrary latitude (θ = 0° is not at equator). Parameters: J set but with $g^* = 0.2, f_0 = 2\Omega_J$. Resolution: R4. Initial state: geostrophic Gaussian vortex with H_0 = 15 km, $\delta\lambda$ = 12°, $\delta\theta$ = 4°, λ_0 = 0°, θ_0 = 0°. Properties: c = 0, L_R = 640 km.

tially 22½° apart in longitude, one of which has twice the amplitude of the other. The stronger vortex catches the weaker vortex in about 500 days and absorbs over half its energy during the first encounter. Later it catches and absorbs the residual and tail vortices, but this takes considerable time. Although anticyclones merge completely, they require more than one encounter to complete the process. The degree of merging depends on the interaction time scale: similar vortices propagate at similar speeds and are more likely to merge completely in one encounter than dissimilar vortices traveling at different speeds. The encounters produce complex amplitude changes but soliton-like phase shifts.

5. Analysis of midlatitude vortices

Further insight into the dynamics of midlatitude vortices can be gained by evaluating their steady-state geostrophic potential-vorticity (GPV) balances. These reveal what processes are active and in what regimes the vortices lie. By examining vortices of different size, we find that stability occurs for a wide range of scales and balances. When the GPV terms in (6)–(8) are calculated using a high resolution and the Sadourny (1975) scheme, they balance precisely. Furthermore, we find that the subgrid diffusion of momentum makes a significant contribution but that for height does not. Table 3 gives the amplitudes of the main processes and shows how their balance changes with vortex size. All of the vortices have winds of the order of 15 m s^{-1}.

a. *Large-vortex dynamics*

Figure 11 gives the important GPV terms for the large, stable (M1) vortex discussed in §4a. From left to right, the columns contain the geostrophic, the primary ageostrophic, and the secondary ageostrophic terms. The steepening-twisting field in frame (c), evaluated by subtracting the translation from the geostrophic divergence, contains two terms: $-H^{-1}c_\beta(y)\eta\eta_{x'}$, describing the steepening and the nonlinear twisting; and $(c_\beta{}^0 - c_\beta(y))\eta_{x'}$, describing the linear twisting. The nonlinear twisting is negligible in the β-plane analyses and only

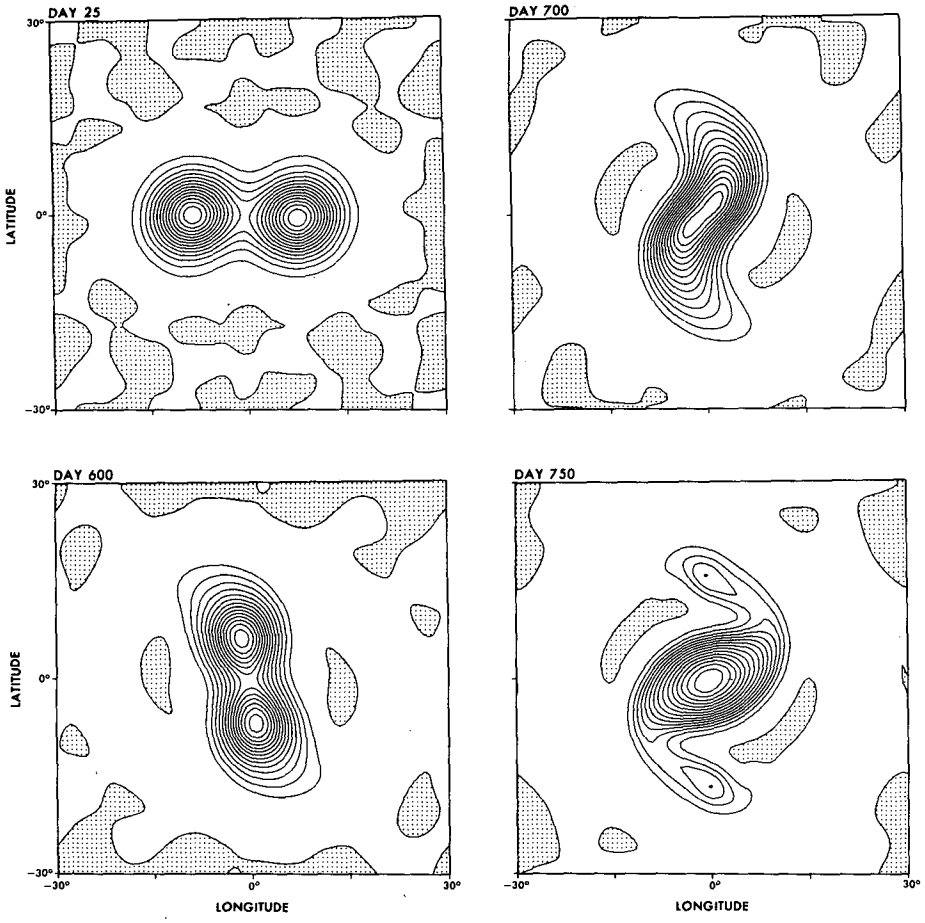

FIG. 7. The f_0-plane solution F2: Interaction of two touching anticyclones. Height η has CI = 0.5 km and axes relative to an arbitrary latitude. Parameters: J set but with $g^* = 0.2, f_0 = 2\Omega_I \sin 30°$. Resolution: R4. Initial state: two identical geostrophic Gaussian vortices with $H_0 = 7.5$ km, $\delta\lambda = 4°$, $\delta\theta = 4°$, centered at $\lambda_0 = \pm 8°$, $\theta_0 = 0°$.

influences very large storms. The ageostrophic divergence in frame (f) equals the sum of the dispersion, advection, and diffusion terms in frames (d), (e), (h), (i) and balances $(h_t + \nabla \cdot h\mathbf{v}^g)$.

The steepening-twisting in Fig. 11c is significantly weaker on the poleside because of the large decrease in $c_\beta(y)$ with latitude, and this makes the vortex asymmetric. The asymmetric steepening also splits the vortex into core and collar regions separated by strong vorticity gradients (Fig. 11g). The collar vorticity is stronger on the west side because the ζv^g term in the vorticity equation

$$\zeta_t + \frac{1}{f} J(h, \zeta) - \frac{\beta}{f} \zeta v^g = -\{\beta v^a + (f + \zeta)\nabla \cdot \mathbf{v}^a\}, \quad (29)$$

increases ζ in the west and decreases it in the east.

The ageostrophic divergence in Fig. 11f counters the changes forced by the steepening-twisting, the largest term in the balance (Table 3). Despite its smooth quadrapole form—a symptom of vortex ellipticity, according to (18)—the ageostrophic divergence is made up of four complex fields having two scales of variation. In the core, the vorticity advection and the dispersion combine to balance the steepening-twisting (Fig. 11e,d,c). In the collar, small-scale variations occur and a strong dispersion balances a strong vorticity advection and a weak kinetic-energy advection. The dispersion field $(-h\zeta_t)$ follows the vorticity Jacobian rather than the vorticity itself and is thus a response to, not a cause of, the generation of small-scale motion. The vorticity diffusion in Fig. 11i is needed to control the small-scale mixing in the western collar.

This large M1 vortex is deceptive: a complex dynamical structure, one not described by existing theory, underlies its smooth height field. As suggested by the scale analysis in §4a, the vortex may be classified as having PG_2 dynamics (see WY84, Table 1) because steepening dominates, but other processes and scales are present. Asymmetry in the propagation produces an advection that prevents a KdV dynamics in the core and forces a QG dynamics in the collar. When steep-

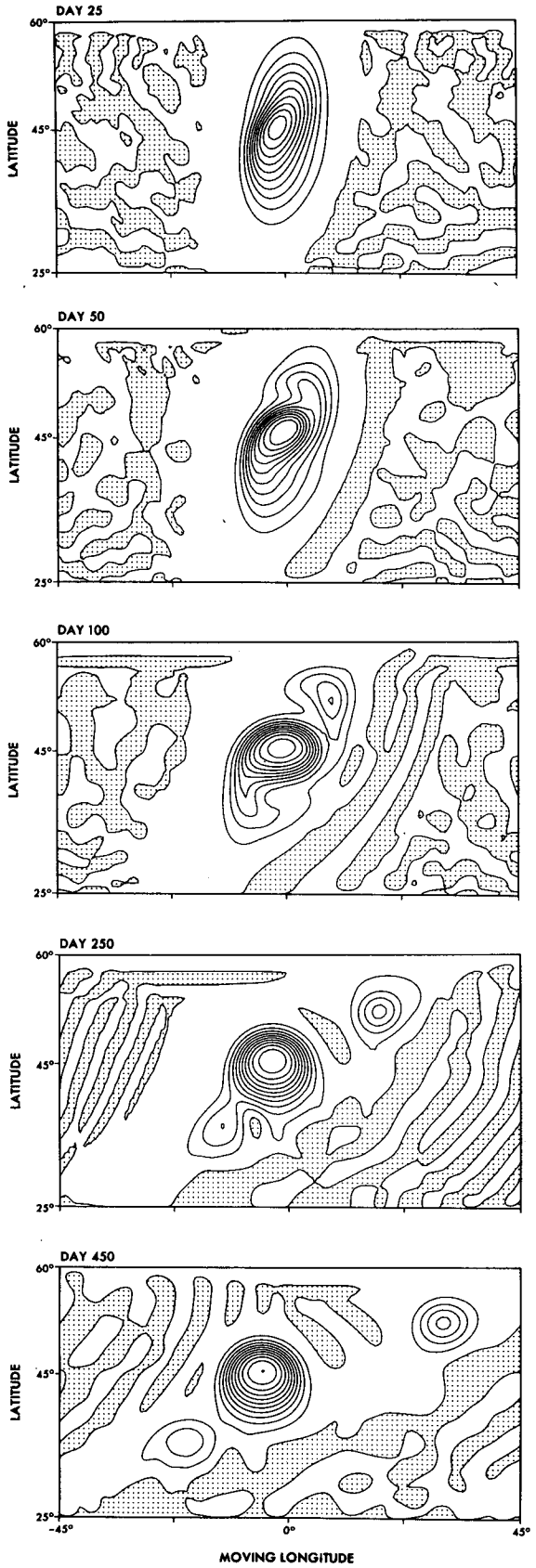

FIG. 8. Midlatitude solution M3: Adjustment of a latitudinally elongated anticyclone. Height η has CI = 1 km and axes moving at $c_a = -1.9$ m s^{-1}. Resolution: R3. Initial state: geostrophic Gaussian vortex with $H_0 = 10$ km, $\delta\lambda = 4°$, $\delta\theta = 6°$, $\lambda_0 = 0°$, $\theta_0 = 45°$.

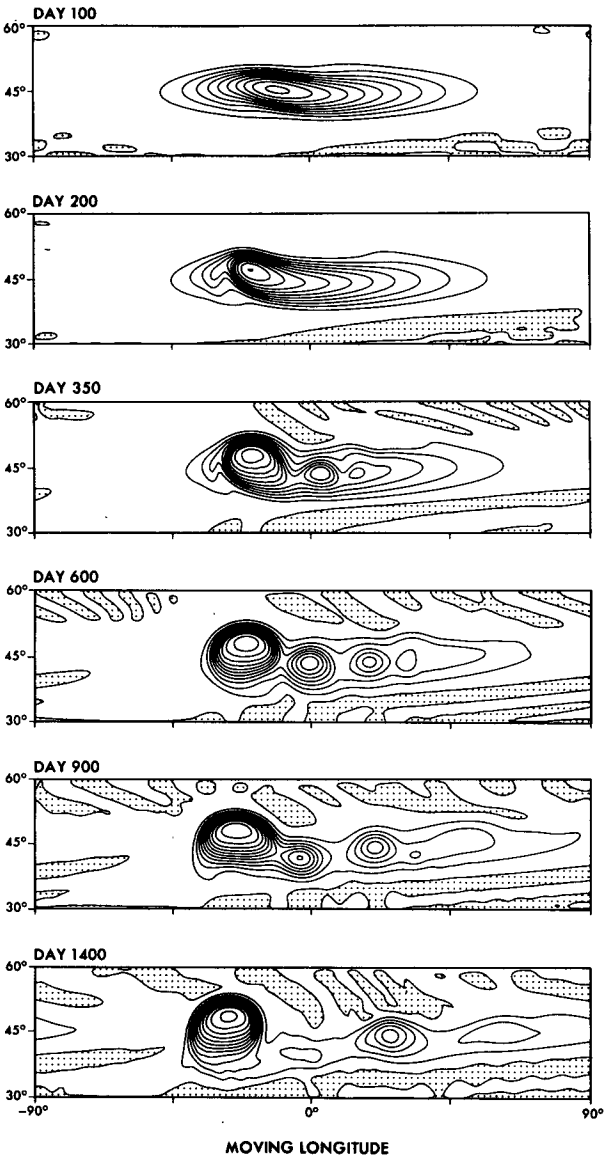

FIG. 9. Midlatitude solution M4: Adjustment of a longitudinally elongated anticyclone. Height η has CI = 1 km and axes moving at $c_a = -1.9$ m s^{-1}. Resolution: R3. Initial state: geostrophic Gaussian vortex with $H_0 = 10$ km, $\delta\lambda = 24°$, $\delta\theta = 3°$, $\lambda_0 = 0°$, $\theta_0 = 45°$.

ening is removed from such a vortex, as in the P3 solution in Fig. 2c, the remaining processes weaken and develop the simple elliptic-vortex forms given by (17), (18). However, the M1 vortex is too large, too close to the limiting size to have a simple balance and to be a good guide to vortex dynamics.

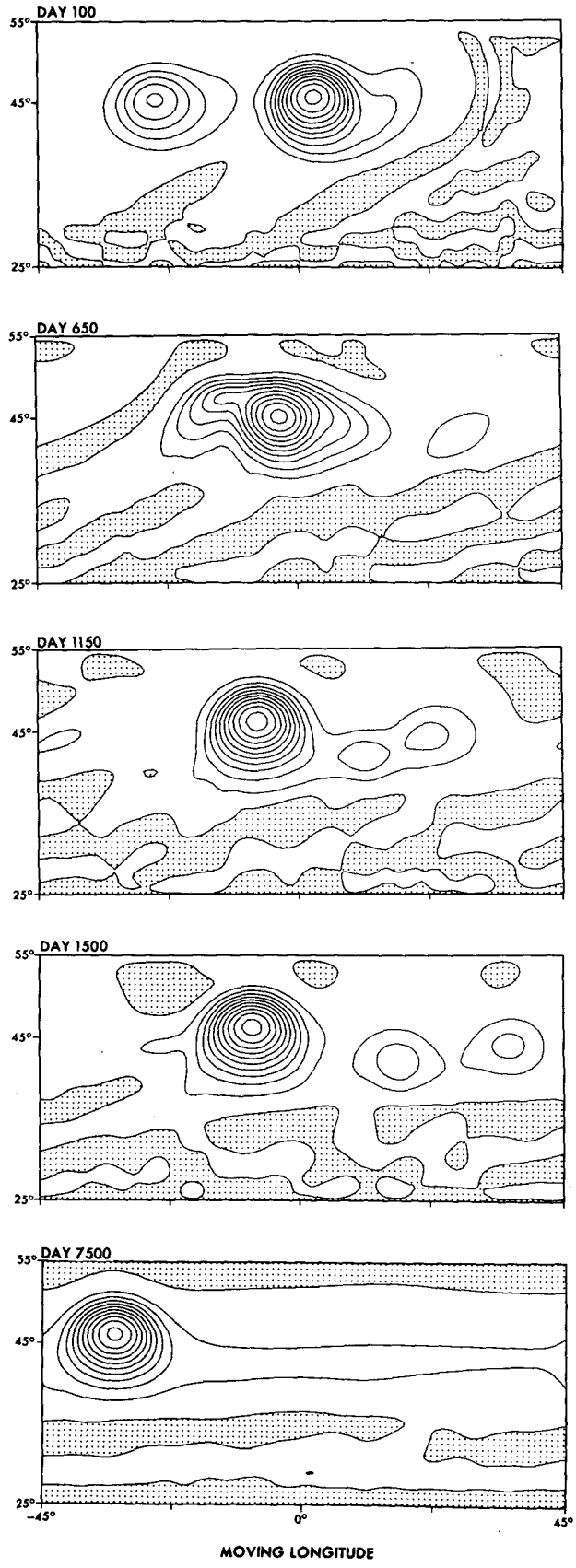

b. *Medium-vortex dynamics*

The stable, long-lived M6 anticyclone in Fig. 12 is half the size of M1 and has a much simpler, single-scale dynamics because of its symmetry and its concentrated core. The dispersion, the strongest process in Table 3, appears to force the dynamics and is balanced by the vorticity advection and, to a lesser extent, by the steepening-twisting (Fig. 12d,e,c). Latitudinal asymmetries caused by the $c_\beta(y)$ variation are apparent in some processes but are secondary. Because ζ parallels h so closely, the vorticity advection reveals a higher-order component $-\zeta J(h, f^{-2})$ that prevents exact radial symmetry and has a dipole distribution like the v field (Fig. 12e).

This balance places the M6 vortex in the modified IG regime described by (11). Although the vortex shape, size, and speed are close to those prescribed by the Rossby-KdV equation, the strong vorticity advection prevents a simple KdV dynamics from operating, even during nonencounter phases. Furthermore, the dispersion and advection are almost as strong as the translation and this reduces the validity of separating processes with slow and fast time scales, as is done in KdV and IG theories. Other calculations show that vortices midway in size between M1 and M6 and initially in a Rossby-KdV balance are also nearly radially symmetric. Strong asymmetries develop only near the M1 scale.

c. *Small-vortex dynamics*

Halving the size of the M6 anticyclone moves it into the QG regime and gives the M7 vortex of Fig. 13. At this scale both cyclones and anticyclones are stable in the sense that they do not collapse immediately into waves, but are unstable in the sense that they migrate poleward or equatorward. Small (QG) vortices tend to move to latitudes where the ambient potential vorticity f/H matches their initial potential vorticity, but larger (IG, PG) vortices such as M1, M6 do not migrate because they can define their own local q gradient. Large anticyclones are stable when they possess a barotropically unstable q gradient in their easterly flow region, suggesting that a vortex is a form of contained instability.

The M7 anticyclone propagates 120° westward and migrates 3° equatorward in 150 days, while losing amplitude and developing a strong core and a trailing envelope (Fig. 13a,g). The dispersion and vorticity advection dominate the balance to give the vortex a QG dynamics (Table 3). The inertia–gravity waves seen in

FIG. 10. Midlatitude solution M5: Interaction of two unequal anticyclones. Height η has CI = 1 km and axes moving at $c_a = -1.9$ m s^{-1}. Resolution: R3. Initial state: Two geostrophic Gaussian vortices with $\delta\lambda = 6°$, $\delta\theta = 3°$, $\theta_0 = 45°$ and (i) $H_0 = 10$ km, $\lambda_0 = 0°$; (ii) $H_0 = 5$ km, $\lambda_0 = -22.5°$.

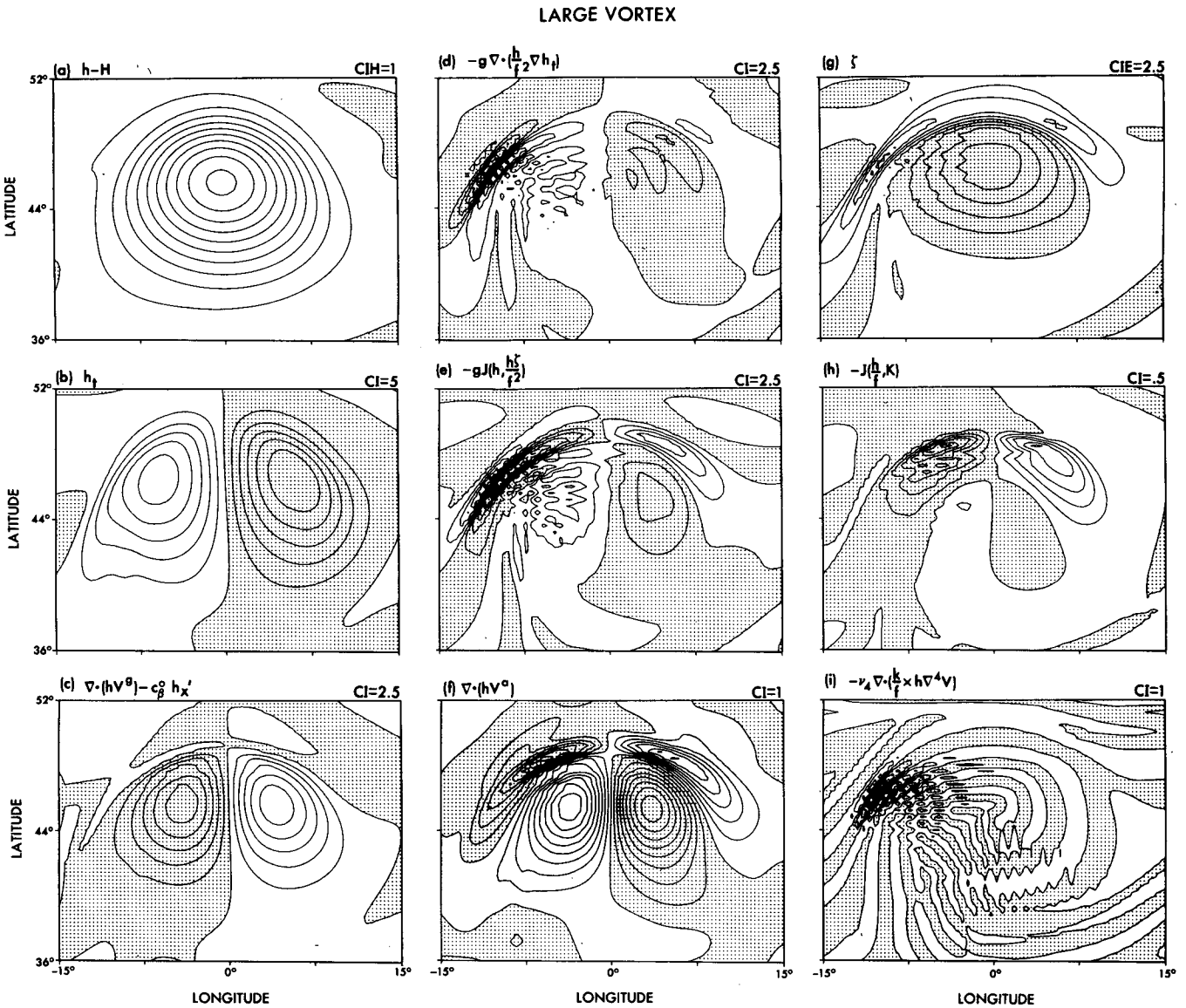

FIG. 11. Analysis of M1 solution: GPV components for a large anticyclone, after 400 days. Contouring: CI, CIH, CIE units are 10^{-2} cm s^{-1}, km, 10^{-6} s^{-1}. Resolution: R6. Prediction domain: $\lambda = \pm 22.5°$, $\theta = 29°$–$53°$. Initial state (as Fig. 4): geostrophic Gaussian vortex with $H_0 = 10$ km, $\delta\lambda = 6°$, $\delta\theta = 3°$, $\theta_0 = 45°$. Data recentered. Notation: $c_\beta^0 = c_\beta(45°)$, $x' = x\cos(45°)$.

the height tendency are generated by the migration but, because of their high frequency, they do not interfere with the internal vortex balance (Fig. 13b). Migration is essential to the partial stability of QG storms (McWilliams and Flierl, 1979).

When the vortex size is halved yet again, its radius

TABLE 3. Approximate amplitudes of processes in various GPV balances; for height tendency, propagation, steepening-twisting, ageostrophic divergence, dispersion, advection Jacobians of vorticity and kinetic energy. Units: 10^{-2} cm s^{-1}. Values in parentheses relate to collar region.

Vortex	h_t	P	$S+T$	$\nabla\cdot(hv^a)$	D	J_ζ	J_K	Type
M1 (Fig. 11)	25	20	13	8 (6)	3 (10)	5 (15)	2	Large
M6 (Fig. 12)	20	20	7	5	15	12	1	Medium
M7 (Fig. 13)	20	15	3	15	50	50	6	Small
M8 (not shown)	40	20	4	40	250	400	150	Very small
P3 (Fig. 2c)	15	15	1	1	1	1	0.1	Linear h_t
L3 (Fig. 23)	150	100	80	50	70	30	25	In $u_J(\theta)$

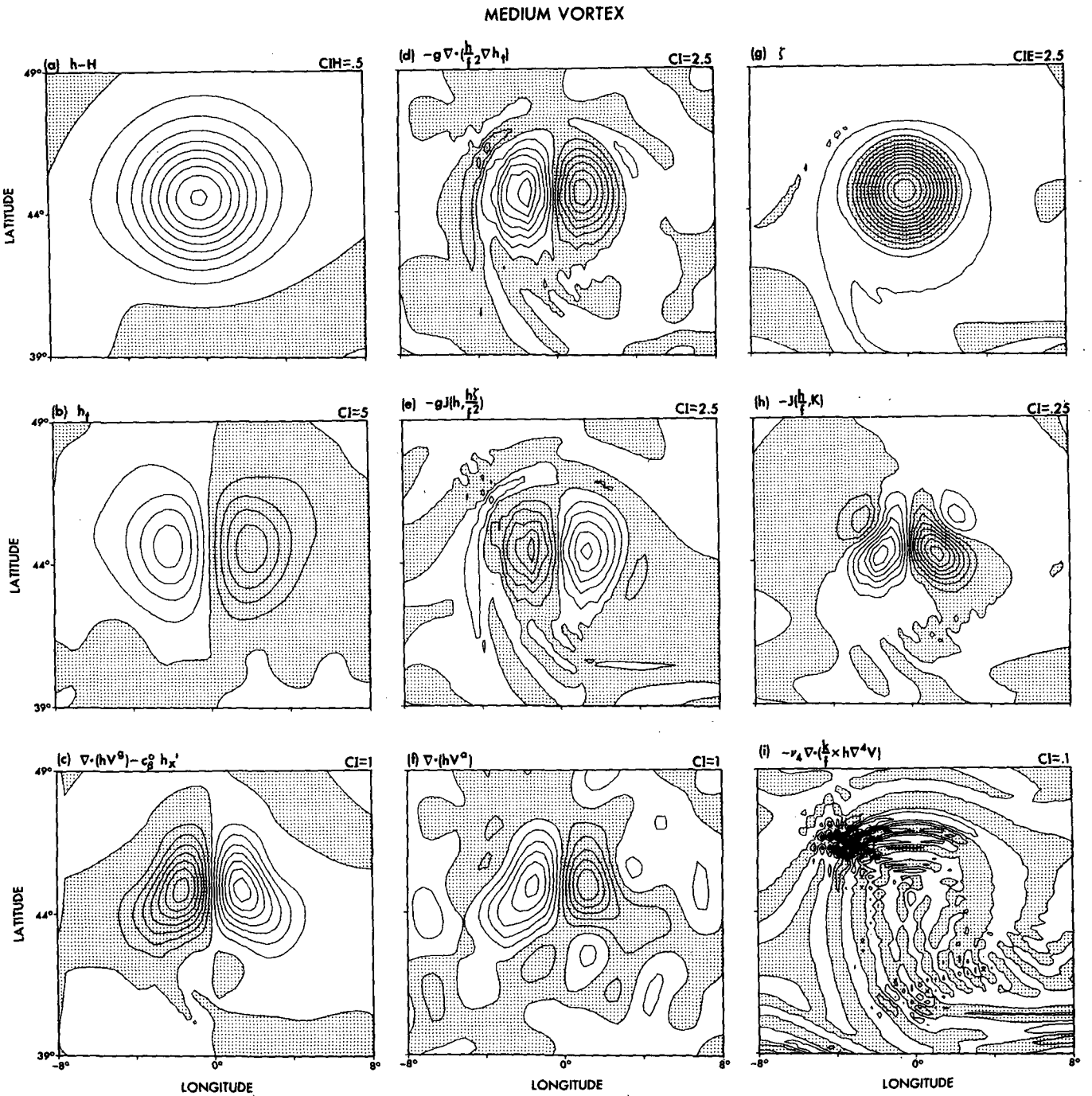

FIG. 12. Midlatitude solution M6: GPV components for a midsize anticyclone, after 550 days. Contouring: CI, CIH, CIE units are 10^{-2} cm s^{-1}, km, 10^{-6} s^{-1}. Resolution: R7. Prediction domain: $\lambda = \pm 16°$, $\theta = 35°$–$51°$. Initial state: geostrophic Gaussian vortex with $H_0 = 5$ km, $\delta\lambda = 2°$, $\delta\theta = 1.5°$, $\theta_0 = 45°$. Data recentered. Notation: $c_\beta^0 = c_\beta(45°)$, $x' = x\cos(45°)$. Properties: $c = -1.7$ m s^{-1}.

then matches the deformation scale L_R. Such an anticyclone (M8) behaves just like M7 but has a simpler dipole dispersion and advection (not shown, but see Table 3). Because of its strong winds, the kinetic-energy advection becomes important and gives the very small vortex a modified QG balance.

6. Vortices at the equator (no zonal flow)

We now turn to the more specific type of vortex that occurs at the equator to see if the form prescribed for it by Boyd (1980) is stable and soliton-like. If it is, then its dynamics is fully defined and needs no further anal-

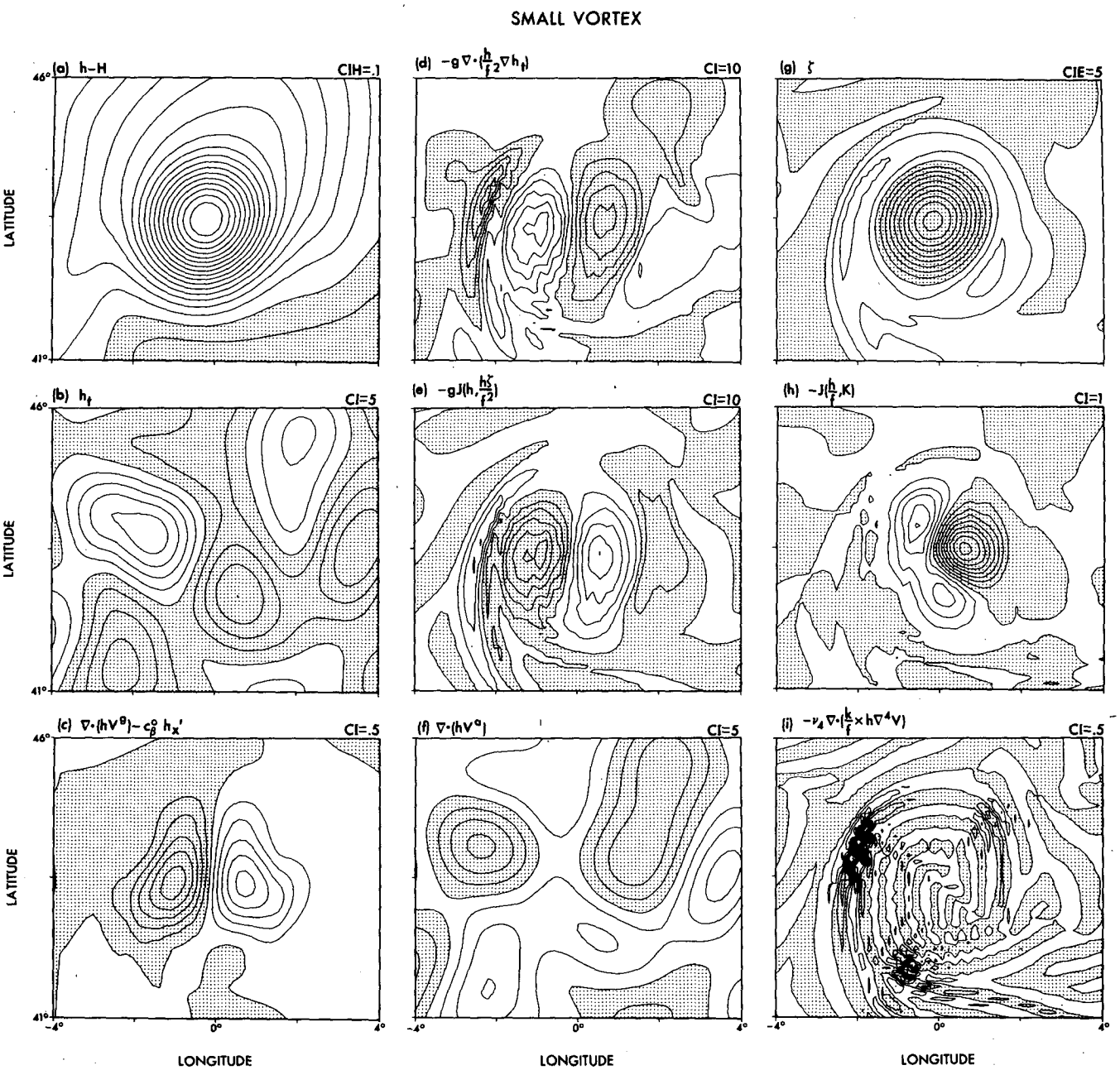

FIG. 13. Midlatitude solution M7: GPV components for a small anticyclone, after 150 days. Contouring: CI, CIH, CIE units are 10^{-2} cm s^{-1}, km, 10^{-6} s^{-1}. Resolution: R8. Prediction domain: $\lambda = \pm 6.75°$, $\theta = 40°$–$48°$. Initial state: geostrophic Gaussian vortex with $H_0 = 2$ km, $\delta\lambda = 1°$, $\delta\theta = 0.75°$, $\theta_0 = 45°$. Data recentered. Notation: $c_\beta^0 = c(45°)$, $x' = x\cos(45°)$. Properties: $c = -1.4$ m s^{-1}.

ysis. These solutions are needed to help us understand the role of zonal currents in stabilizing low-latitude vortices in §7.

a. Long-lived anticyclones at $\theta_0 = 0$

The 10-year progression of the $n = 1$ solitary wave in Fig. 14 illustrates the stability and probable permanence of such modes. The anticyclone evolves slightly from the initial state defined by Boyd's (1980) zero-order solutions but it does so in keeping with Boyd's (1984) higher-order solutions for strong vortices. The amplitude was chosen to make the vortex comparable in size and strength with the mid- and low-latitude vortices discussed in other sections. The vortex propagates westward at -65 m s^{-1}, considerably faster than the linear wave speed ($c = -c_g/3 = -54$ m s^{-1}) but in keeping with the amplitude factor $V\alpha_n/3$ in (28).

The height extrema in equatorial vortices (η reaches

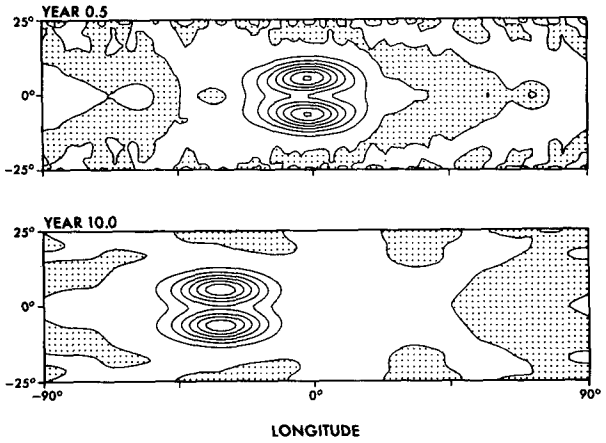

FIG. 14. Equatorial solution E1: Longevity of an $n = 1$ anticyclone. Height η has CI = 0.25 km. Resolution: R1. Initial state: Boyd's v_n^0, η_n^0 with $n = 1$, $V = 0.28$, α_1 and γ_1 as in Table 2, dimensioned by c_g and H. Properties: $c = -65.0$ m s^{-1}, $c_g/3 = 54$ m s^{-1}, $L_R = 5700$ km.

1.5 km in Fig. 14) are considerably smaller than in midlatitude storms of comparable kinetic energy. The corresponding (u, v, w) velocities reach peaks of (40, 7, 0.004) m s^{-1}. The zonal flow is mainly easterly and strongest at the equator. The height and flow fields are the same as if two midlatitude vortices, one in each hemisphere, touched at the equator to produce a modon (Boyd, 1984). Although the $n = 1$ modes, some highly nonlinear, can exist for a wide range of amplitudes, the $n = 3, 5, 7, \cdots$ modes remain stable only for the narrow range prescribed by Boyd's theory.

When an anticyclone of order n is overly strong, it stabilizes itself by shedding an anticyclone of order $n - 2$, something the $n = 1$ mode cannot do. Thus, an overly strong $n = 5$ mode splits into a weaker $n = 5$ mode and an $n = 3$ mode. Anticyclones with even n values are unstable because their α_n vanish and the KdV equation reduces to linear dispersion (Boyd, 1980).

b. *Vortex interactions at $\theta_0 = 0$*

The interactions between two $n = 1$ equatorial anticyclones, one having 2.5 times the amplitude of the other, are characteristic of solitons: the amplitudes are maintained and the phases are shifted during encounters at days 700 and 900 (Fig. 15). By exchanging identities the stronger vortex jumps ahead approximately 10° in longitude and the weaker one falls behind. No simple latitudinal changes are detected. The reference frame for this $\eta(\lambda, t)$ plot moves at $c_a = -62$ m s^{-1} to freeze the weaker vortex.

When the equatorial vortices have different latitudinal forms, they obey different scaling constraints and different KdV equations and need not interact like solitons. Figure 16 illustrates the stability and interaction of the $n = 3$ and $n = 5$ solitary waves over a period allowing multiple encounters. Initially, the two vortices are equally long, lie at $\lambda_0 = 0$, and combine into a high centered at $\theta = 10°$. The individual anticyclones soon emerge because of their distinct drift rates (-23 and -15 m s^{-1}) and are fully separated at days 180 and 460. The vortices lie at the same longitude again at days 300 and 600 and recreate a single storm. The encounters weaken the $n = 5$ mode but strengthen the $n = 3$ mode, thereby transferring energy equatorward. Interactions between the different-order modes produce quasi-soliton exchanges and recurrences because the encounter time is too short to allow wave–wave interaction. Similar mixed-mode interactions have been studied theoretically for other types of solitary wave by Redekopp and Weidman (1978) and Malanotte-Rizzoli (1982).

7. Low-latitude vortices in stable currents

Low-latitude anticyclones (such as the GRS) are only stable when zonal currents exist to eliminate the generation and propagation of the highly dispersive equatorial modes. The following solutions show that a low-latitude anticyclone can be stabilized by an equatorial westerly jet that limits the external wave propagation and by a subtropical easterly jet that modifies the internal vortex dynamics.

a. *Linear theory: $u_0(y)$ effect on eigenfunctions*

The Jovian zonal flow configuration $u_0 = u_J(y)$ consists of a strong westerly jet (W_1) at the equator, an adjacent easterly current (E_1), and a westerly jet (W_2)

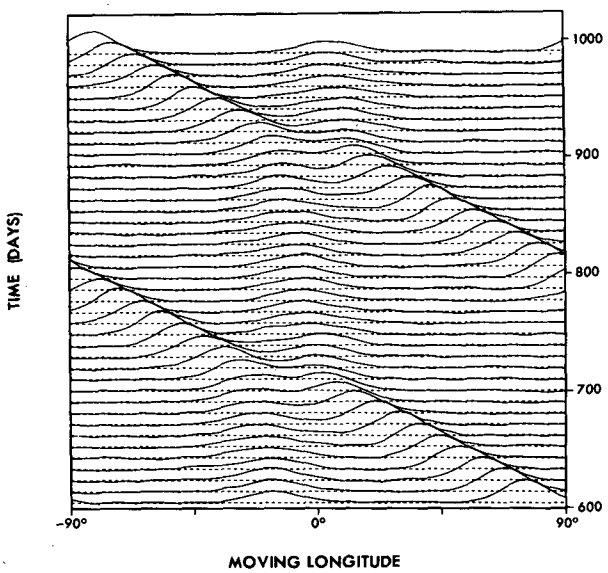

FIG. 15. Equatorial solution E2: Interaction of two unequal $n = 1$ anticyclones. Height $\eta(\lambda, t)$ at $\theta = 5°$ has axis moving at $c_a = -62$ m s^{-1}. Resolution and domain as Fig. 14. Initial state: Boyd's v_n^0, η_n^0 with $n = 1$ and (i) $V = 0.188$, $\lambda_0 = -45°$, (ii), $V = 0.471$, $\lambda_0 = +45°$, dimensioned by c_g and H. Properties: $c = -61.5$ m s^{-1} and -72.5 m s^{-1}, $c_g/3 = 54$ m s^{-1}.

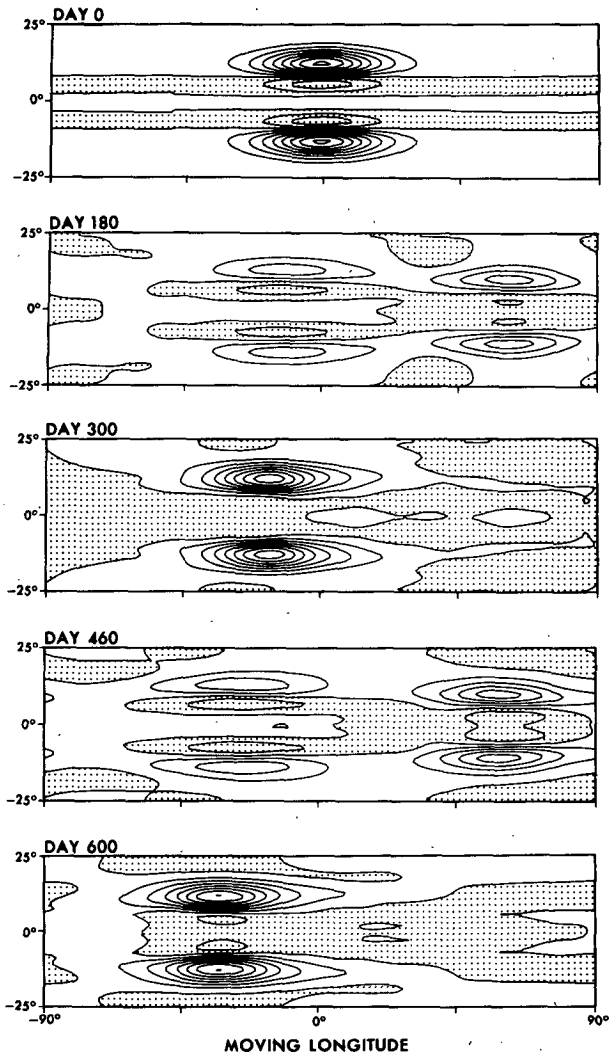

FIG. 16. Equatorial solution E3: Interaction of $n = 3$ and $n = 5$ anticyclones. Height η has CI = 0.2 km and axes moving at $c_a = -14.5$ m s^{-1}. Resolution: R1. Initial state: Boyd's v_n^0, η_n^0 with (i) $n = 3$, $V = 0.05$; (ii) $n = 5$, $V = 0.03$, both centered at $\lambda_0 = 0°$, and dimensional by c_g and H. Properties: $c_g/7 = 23.1$ m s^{-1}, $c_g/11 = 14.7$ m s^{-1}.

poleward of that (Fig. 17). Associated with the currents are the geostrophic height $h_0(y)$, the potential vorticity $q_0(y) = (f - u_{0y})/h_0$ and its gradient $q_{0y} = (\beta - u_{0yy} + fq_0u_0g^{-1})/h_0$. The q_{0y} profile changes sign in the easterly, indicating that the current may be barotropically unstable (Ripa, 1983). Such easterlies are used in §8, but in this section they are weaker and stable. Both u_0 and h_0 can affect wave propagation: u_0 by advecting short waves and h_0 by altering the local c_β of long waves.

The zonal currents influence vortex stability mainly by modifying the propagation characteristics of the eigenfunctions. A detailed view of the influence of the equatorial westerly is given by solving the linearized SL equations for waves in the presence of the current $u_0(\theta) = U[1 + (\theta/\delta\theta)^8]^{-1}$, using the spectral eigenvalue method described by Ripa and Marinone (1983). The resulting eigenfunctions in Fig. 18 show that the jet expells the high-k, low-n modes from the equatorial region while reshaping the low-k, low-n modes there. Clearly, only the largest-scale disturbances can occur at the equator when the westerly jet is strong, in keeping with the concept of scale-dependent turning latitudes. The low-latitude easterly jet influences vortex stability mainly by suppressing the generation of these large modes; see §7c.

b. *Vortex plus equatorial jet*

To clarify the role of the three low-latitude jets on stability, we examine vortices in the presence of one or more of the currents at a time. We find that only the equatorial westerly is vital to vortex stability, but that the easterly plays a useful support role. Figure 19 illustrates the longevity the equatorial westerly gives to a low-latitude anticyclone. The 90° longitudinal domain of this L1 solution, however, excludes the longest equatorial modes and these, as the next solution shows, can be important.

When the domain is extended to 180°, the vortex appears to behave initially like an $n = 5$ solitary wave and releases $n = 3$ and $n = 1$ solitary waves that elongate the anticyclone and create a weak disturbance at the equator (Fig. 20). By day 1700 the vortex has adjusted and the equatorial disturbance has strengthened sufficiently to detatch itself and develop into a distinctive $n = 1$ equatorial anticyclone that strongly decelerates the local zonal flow by 40 m s^{-1} (Fig. 21). The equatorial storm propagates westward, despite the jet, at speeds varying from -16 to -19 m s^{-1} and occasionally interacts with the low-latitude vortex moving at -12 m s^{-1}. In their first reunion, at day 2000, the two have a recurrence encounter in which the initial state appears to be fully recovered. The equatorial vortex reemerges 200 days later and gradually, through successive encounters, extracts further energy from the low-latitude anticyclone to become predominant.

The zonal flow influences the generation of equatorial anticyclones by controlling the extent to which low-latitude vortices project onto equatorial modes of comparable order and phase speed. When the equatorial jet is strong ($W_1 \geq 100$ m s^{-1}) the low-latitude vortex generates one equatorial anticyclone; when the jet is moderate ($W_1 \sim 75$ m s^{-1}) it creates two. When the jet is weak ($W_1 < 50$ m s^{-1}), however, the low-latitude vortex decays, as in the current-free case of Fig. 3. For a low-latitude vortex to be completely stable the very long waves that it generates at the equator must be eliminated, either by maintaining the westerly jet at a fixed amplitude or by including the easterly jet—as in the next case.

c. *Vortex plus westerlies and easterly*

When all three currents are present, a vortex embedded in the anticyclonic zone lasts indefinitely, as the

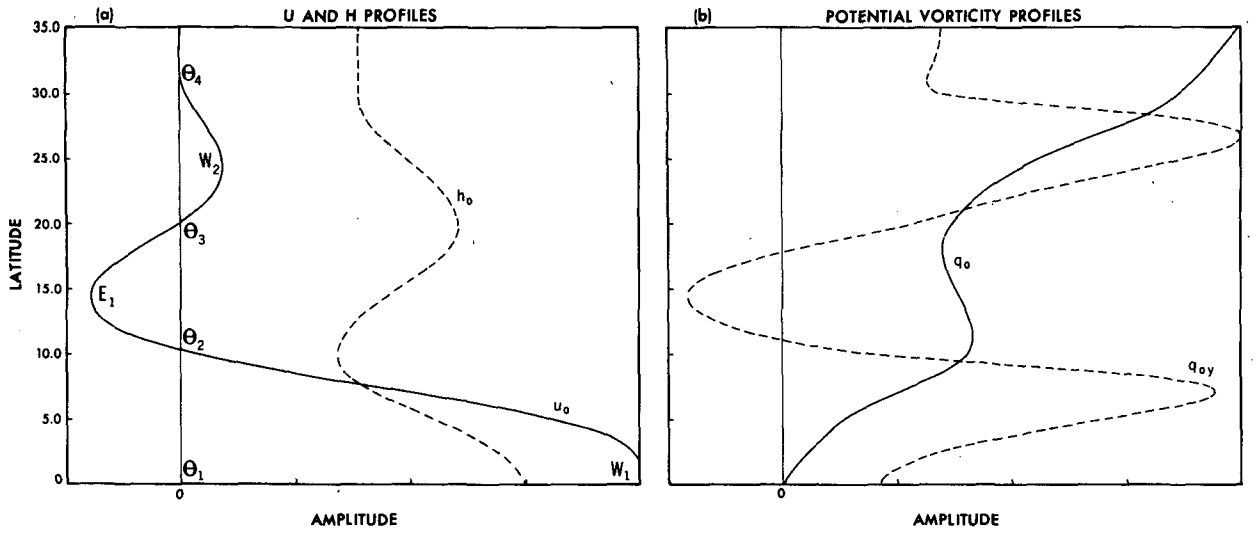

FIG. 17. Profiles of the basic zonal flow, geostrophic height and potential vorticity; where $q = (f + \zeta)/h$. The westerly and easterly jets, denoted by their amplitudes W_1, E_1, W_2 and extending over latitudes θ_1 to θ_4, are created from patched and smoothed individual $\sin\theta$ or $\cos\theta$ representations; the equatorial jet is flat from $\theta = 0°$ to $3°$ and then has a $\cos\theta$ variation. Resolution: $\Delta\theta = 0.5°$.

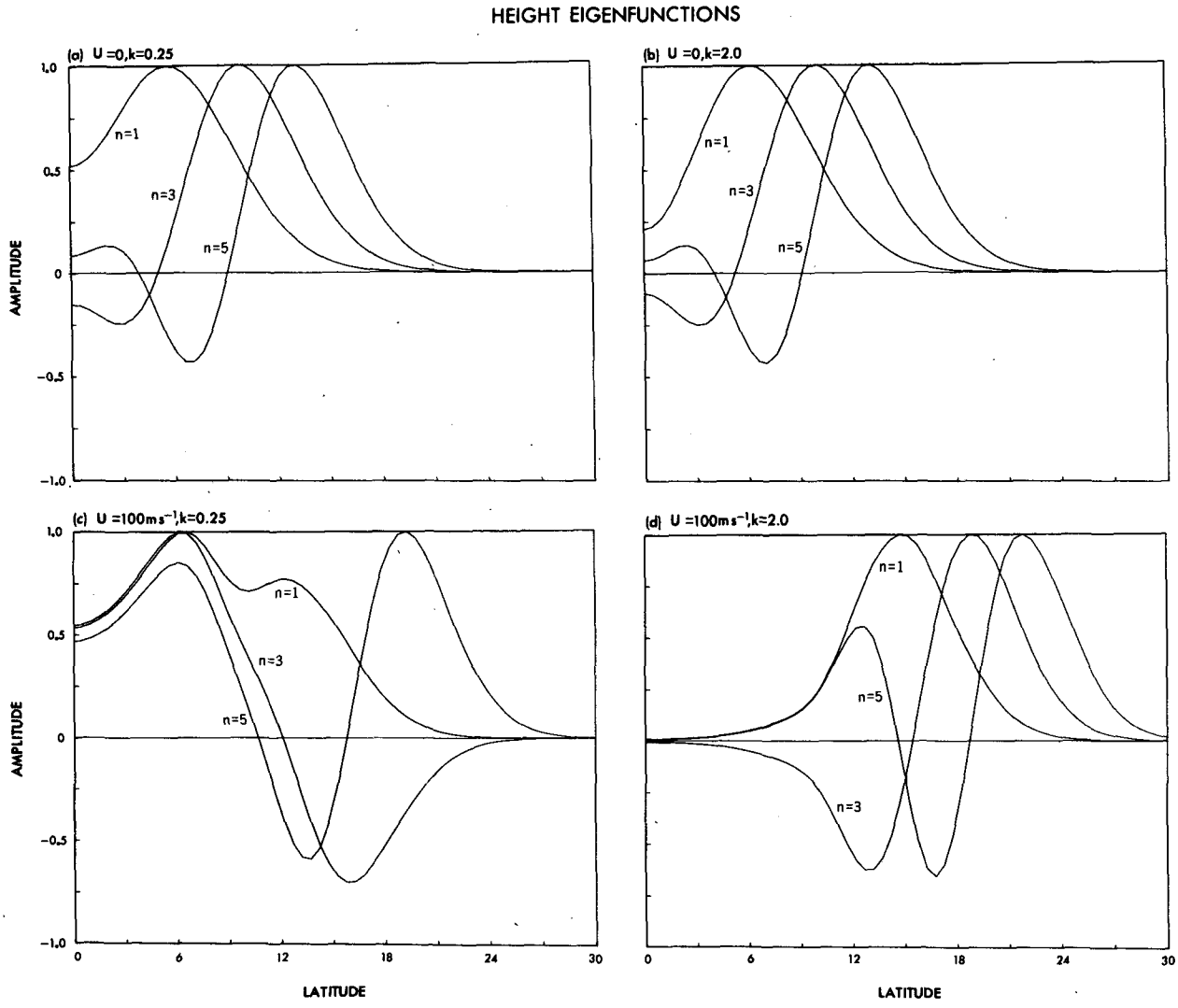

FIG. 18. Modification of the equatorial $n = 1, 3, 5$ eigenfunctions by an equatorial westerly jet: (*a*, *b*) without jet; (*c*, *d*) with jet. Zonal current: $u_0(\theta) = U(1 + \{\theta/\delta\theta\}^8)^{-1}$, $U = 100$ m s^{-1}, $\delta\theta = 8°$. Low and high longitudinal wavenumbers $k = 0.25$ and 2.0 corresponds to lengths of order 10^5 and 10^4 km when redimensioned by $(\beta/c_g)^{1/2}$.

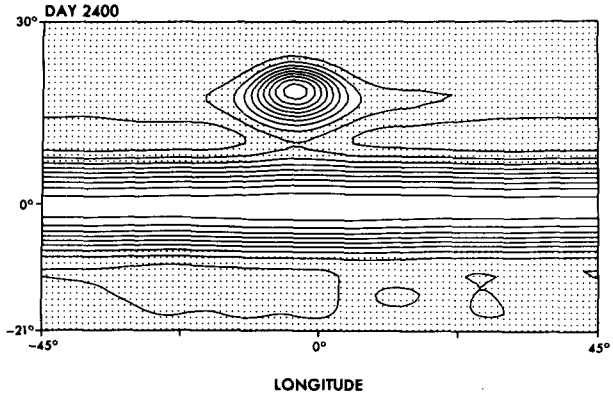

FIG. 19. Low-latitude solution L1: Longevity of an anticyclone in the presence of an equatorial westerly jet, in a short domain. Height η has CI = 1 km. Resolution: R1. Initial state: geostrophic Gaussian vortex with $H_0 = 10$ km, $\delta\lambda = 6°$, $\delta\theta = 3°$, $\lambda_0 = 0°$, $\theta_0 = 20°$, adjacent to a geostrophic jet with $W_1 = 100$ m s^{-1}, $\theta_2 = 10°$. Properties: $c = -11.6$ m s^{-1}, $c_\beta(20°, h) = -7.8$ m s^{-1}, $h(20°) = 8.1$ km.

100-year simulation (involving two million timesteps) in Fig. 22 demonstrates. The vortex and currents maintain their original amplitudes throughout without forcing, but undergo small changes in form. The E_1 and W_2 currents have to be weaker than Jupiter's cloud-level winds to avoid barotropic instability, but the equatorial current has to equal the cloud-level winds to prevent vortex collapse. These different representations suggest that separate dynamical regimes exist in the two planetary regions. If the planet has a Hadley regime near the equator, then the issue of low-latitude vortex stability in the SL system may be irrelevant to Jupiter. A Hadley regime could stabilize vortices more easily but would require a more complex model to describe the process.

The L3 vortex in Fig. 22 is stable because the strong equatorial westerly excludes all but the longest modes from the equatorial zone, and because the height field $h_0(y)$ associated with the easterly current reduces the twisting in the vortex zone and thereby eliminates the generation of the large modes. To see the latter effect, we recall from (2.11) of WY84 that in the presence of currents the idealized IG equation has the form:

$$\xi_t - \xi_x - \xi\xi_x - (1 + u_0)\nabla^2\xi_x + (2y - h_0 - h_{0yyy})\xi_x - J(\xi, \nabla^2\xi) = 0, \quad (30)$$

where $\xi = \eta - h_0$ measures the relative displacement. In the easterly of Fig. 17, h_0 increases uniformly as $+y$ and can easily reduce, remove, or reverse the twisting term in (30). This h_0 factor originates in the $hh_x(f^{-1})_y$ term in (9) and the elimination of twisting is equivalent to basing the propagation speed on the local long-wave speed $c_\beta(h_0) = -gh_0/f^2$ instead of on the mean $c_\beta(H) = -gH/f^2$. The h_0 and f^2 variations can be made to cancel for special currents, just as they can for special $g(\sin^2\theta)$ distributions.

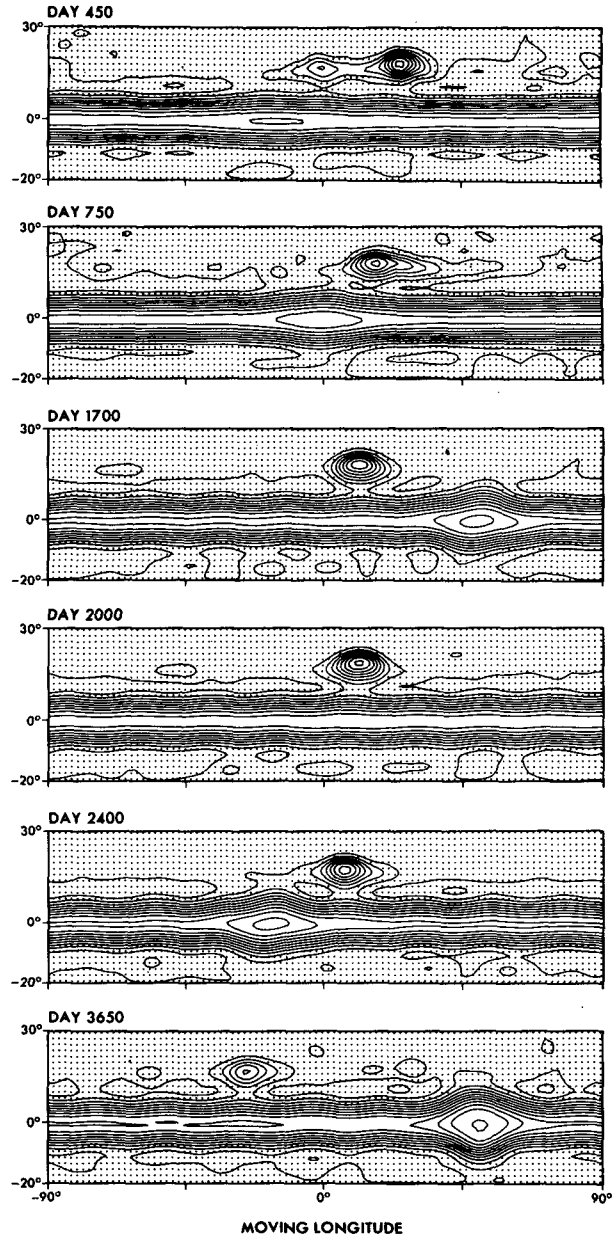

FIG. 20. Low-latitude solution L2: Reduction of a low-latitude anticyclone and the genesis of an equatorial anticyclone in the presence of an equatorial westerly jet. Height η has CI = 1 km and axes moving at $c_a = -12$ m s^{-1}. Resolution: R1. Initial state: as Fig. 19.

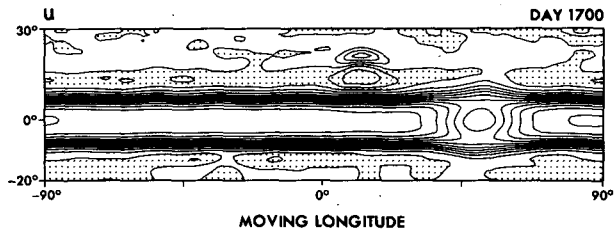

FIG. 21. Low-latitude solution L2: Zonal velocity for the flow in Fig. 20 at Day 1700 has CI = 10 m s^{-1} and shaded easterlies.

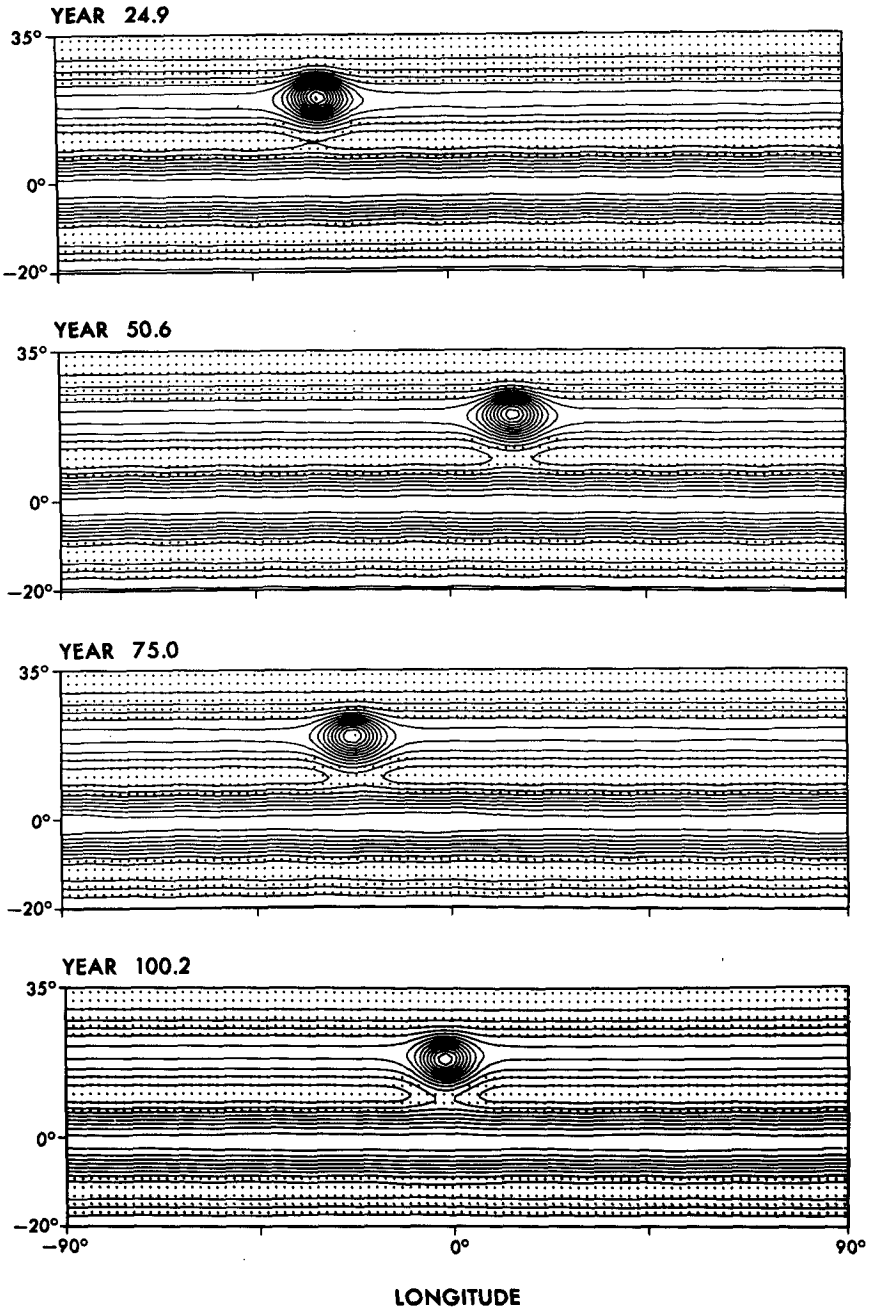

FIG. 22. Low-latitude solution L3: Longevity of an anticyclone in the Jovian jet configuration. Height η has CI = 1 km. Resolution: R1. Initial state: geostrophic Gaussian vortex with $H_0 = 10$ km, $\delta\lambda = 6°$, $\delta\theta = 3°$, $\lambda_0 = 0°$, $\theta_0 = 20°$, embedded in geostrophic $u_J(\theta)$ jets with $(W_1, E_1, W_2) = (100, -15, 10)$ m s^{-1} and $\theta_{1,2,3,4} = (0°, 10°, 20°, 30°)$.

The GPV balance in Fig. 23 shows that the L3 vortex may be classified as having an IG dynamics modified by the kinetic-energy advection. The processes have the same form as for the large M1 midlatitude anticyclone, but their amplitudes have a different priority. In L3 the steepening-twisting is balanced by the dispersion plus some advection to make it more KdV-like than in the M1 case, where the steepening-twisting is balanced by the vorticity advection plus some dispersion. The twisting and the vorticity advection should both be quadrapolar for this elliptic vortex, but only the latter is. This suggests that the twisting has indeed

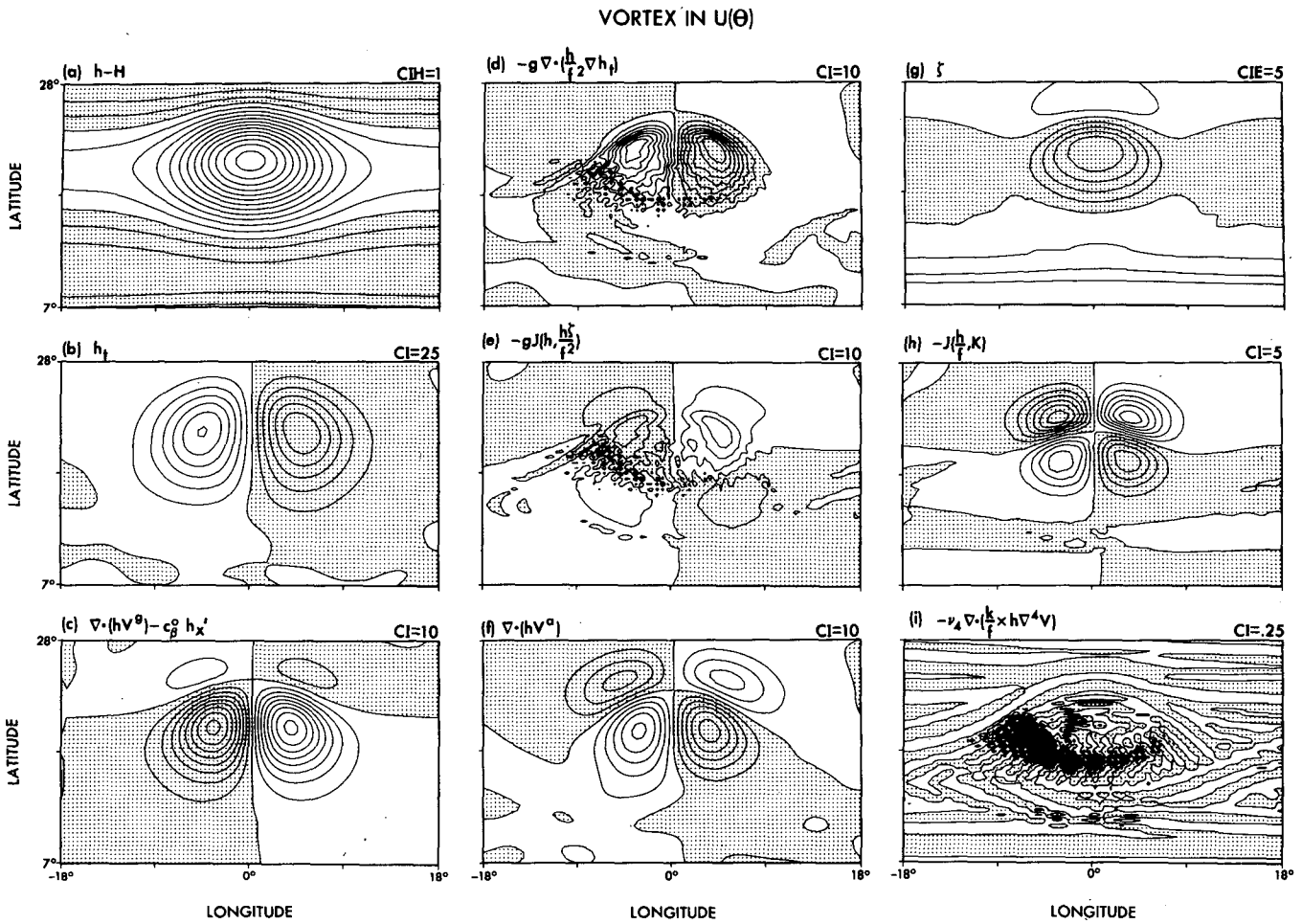

FIG. 23. Analysis of L3 solution: GPV components for a low-latitude anticyclone embedded in zonal currents. Contouring: CI, CIH, CIE units are 10^{-2} cm s^{-1}, km, 10^{-6} s^{-1}. Resolution: R5. Prediction domain: $\lambda = \pm 22.5°$, $\theta = 0°$–$30°$. Initial state: as Fig. 22. Notation: $c_\beta^0 = c_\beta(20°)$, $x' = x\cos(20°)$.

been reduced by the easterly h_0 effect. All terms are stronger in lower latitudes because of their f^{-1} to f^{-3} dependencies, where $f(45°)/f(20°) = 2.1$, (Table 3).

Finally, we note that in the presence of stabilizing currents, low-latitude vortices merge during encounters. Thus, the jets effectively extend the midlatitude regime towards the equator (cf. Petviashvili, 1983).

8. Vortex genesis

We now examine how Rossby vortices are generated by shear instability and by stochastic eddy forcing. To help understand the origin and uniqueness of Jupiter's GRS, we confine our calculations to low latitudes and concentrate on finding the simplest, most general conditions under which *single* vortex states are produced. We find from a variety of calculations that the vortex number depends primarily on the interaction history, that the factors controlling the linear instability—the strength of the easterly, the width of the anticyclonic zone, the Rossby radius—are secondary. The following examples illustrate how similar (single) vortex states can emerge in dissimilar environments and how dissimilar (single, double) vortex states can emerge in similar environments.

a. *Genesis 1: Wave-packet perturbation of broad currents*

The Kuo and Fjortoft criteria, that q_{0y} change sign and that $[u_0 - u_0(y_i)]q_{0y}$ be mainly positive, describe the necessary conditions for the unstable growth of eddy enstrophy and kinetic energy, where $q_{0y}(y_i) = 0$ defines the inflection latitude y_i. Waves of phase speed c become unstable through a quantized meridional propagation between the inflection latitude and the over-reflecting critical latitude at y_c, where $u_0(y_c) = c$ defines the latter, (Lindzen and Tung, 1978). In the SL model the shear instability depends on both $u_0(y)$ and $h_0(y)$ through a q_{0y} gradient that varies as $(\beta - u_{0yy} + u_0 L_R^{-2})$ for midlatitude flows with a small divergence, and as $(\beta - u_{0yy} + u_0 fqg^{-1})$ for equatorial flows and for midlatitude flows with a large divergence (Ripa, 1983). The latter form allows for $O(u_0^2)$ and $c_\beta(h_0 f^{-2})$ variations.

The easterly in Fig. 17 has critical and inflection latitudes near $\theta = 12°$ and $\theta = 18°$ that may provide the confinement needed for instabilities to grow. Linear long waves, however, have coincident y_i and y_c and are probably stable. Thus Rossby vortices based on neutral linear long waves cannot extract energy directly from the basic shear and can only grow through a nonlinear instability or an energy cascade from smaller, unstable waves.

The Genesis-1 calculation shows how a weak wave-packet perturbation added to broad unstable currents evolves through linear growth and nonlinear interaction into a single vortex (Figs. 24, 25). The initial disturbance consists of ten oscillations over 180° of longitude in a $\text{sech}^2\lambda$ envelope. The anticyclonic zone is 10° wide in latitude and has a shear that is 25 m s^{-1} stronger than that in the stable L3 case of Fig. 22. In the initial phase (visible in the v field), small-scale waves grow near the easterly peak and transfer energy northward to the h_0 peak.

The development of the instability only becomes apparent in the height field when closed contours form at day 400 (Fig. 24). The wave packet then grows into a series of vortices of similar size but different strengths. The strongest vortex occurs in the middle of the packet and has a 7-km height by day 700. By day 1200 the current has stabilized and the disturbance has matured into two strong central vortices and three moderate peripheral vortices. From now on, only vortex propagation and interaction occur, and these are fully described by the time section in Fig. 25. The first merger is complete by day 1700 and produces a dominant vortex that absorbs the others during encounters ending at days 2300, 3400, 5500 and 6000. Thus the nonlinear instability produces a single powerful vortex with a 13.5 km height, a 30° length, and a westward drift that exceeds the long-wave speed c_β by 50%.

b. *Genesis 2: Wave-packet perturbation of narrow currents*

The Genesis-2 calculation in Fig. 26 illustrates just how strong a factor the interaction history is in determining the number of vortices. In this solution the anticyclonic zone is narrowed to 8° of latitude but kept centered at $\theta = 20°$ by widening the equatorial jet. The shear is kept strong and is perturbed by a wave packet. The disturbance develops into ten unequal vortices that strengthen and then merge through amplitude or size pairing.

By day 1500 the mergers have reduced the set to one strong, one moderate and two weak vortices. To survive, the moderate vortex must absorb the weak ones before the strong one catches it. By day 2000 the moderate vortex has absorbed one weak vortex and lies equally far from the strong and remaining weak vortex. By day 3100 the moderate vortex has caught the weak one but the large one has halved the gap to 20° and is close on its heels. By day 3950, however, the merger is complete and the strengthened moderate vortex is 30° ahead and safe. The two final vortices have almost the same size and shape and they coexist by becoming evenly spaced and propagating at similar speeds.

The emergence of two vortices in this Genesis-2 case is partly an accident of an evolution that almost results in a single vortex, as a calculation with a slight change in the initial conditions verifies. Note that a weak equatorial anticyclone is also produced.

c. *Genesis 3: Stochastic eddy forcing*

It was shown in a paper on the role of barotropic β-turbulence in the formation of Jupiter's jets (Williams, 1978) that stochastically forced eddies cascade energy to larger scales and, by generating Rossby waves, evolve into an alternating series of zonally aligned easterly and westerly jets. Vortices did not develop because the model was nondivergent and dissipative. The Genesis-3 case in Fig. 27 shows that in a divergent fluid eddies cascade, by wave interactions, into zonal currents and, by eddy mergers, into a single vortex. Vortex merging, not the vorticity source, is the main determinant of vortex states in the SL system. The Genesis-3 solution also shows that large vortices thrive in a turbulent environment and can be made to move eastward.

In setting up the calculation, the eddies are energized by forcing the height field in (3) with a function $F(\lambda, \theta, t)$ whose single Fourier mode has a half wave over $\theta = 20°$ to 30° and ten waves over $\lambda = \pm 45°$, with random longitudinal phases defined by the Langevin equation (15) of Williams (1978). This eddy forcing crudely represents the baroclinic instability of the W_2 jet. A part of the W_2 westerly jet is directly forced via the v_t equation by a term of the form $F_v = fu^F = W_2(y)/\tau$. In the absence of eddies this forcing produces a basic state $fu_{0y} = -g\eta_{0y} + fu^F$ in which waves propagate at a speed $c = u_0 - [\tilde{\beta} - q_0\eta_{0y}]/[k^2 + l^2 + L_R^{-2}]$, where $\tilde{\beta} = \beta - u_{0yy}$. Long waves can be Doppler shifted only if the basic state has an *ageostrophic* component, otherwise the u_0 and η_{0y} contributions cancel. (Note, however, that geostrophic jets can modify long-wave drift at the equator, as in Fig. 20.) Solving the adjustment problem (Charney, 1973; p. 185) for our Jovian parameters shows that this forcing produces a fully ageostrophic basic flow, $u_0 = u^F$, $\eta_0 = 0$, that gives long waves a speed $c = u^F + c_\beta$ and crudely represents the baroclinic component of the westerly jet. In addition, an equatorial jet is imposed to restrict wave propagation into the equatorial zone. No easterly current is forced directly.

In the Genesis-3 solution in Figs. 27 and 28, the weak eddy forcing gradually generates a series of ten cyclones and ten anticyclones that separate out in latitude and propagate uniformly eastward—the rapid random phase variations being filtered out. The anti-

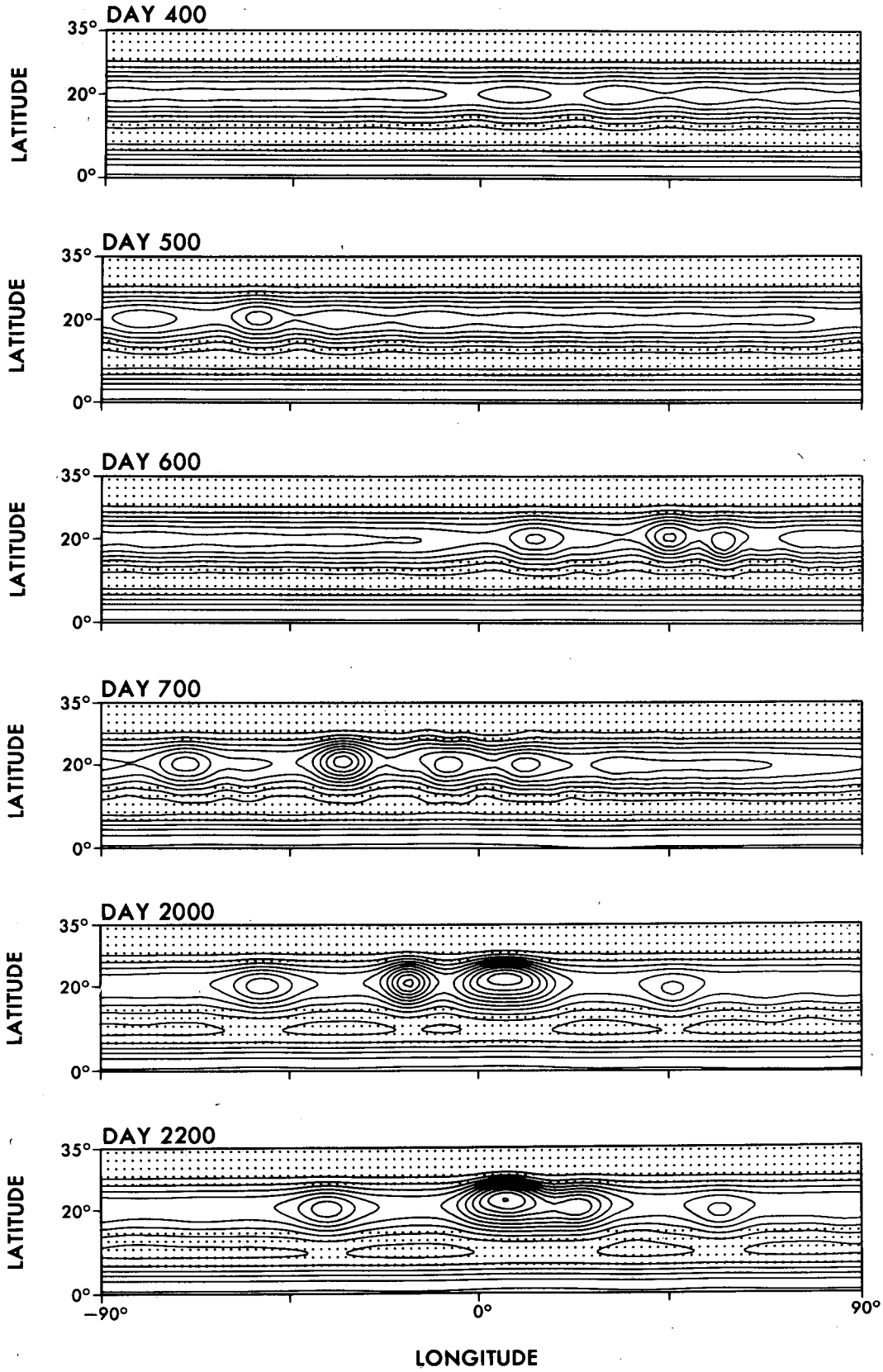

FIG. 24. Low-latitude solution Genesis 1: Generation of a single long-lived anticyclone from a wave-packet perturbation of broad unstable currents. Height η has CI = 1.5 km and axes scaled at 20°. Resolution: R3.

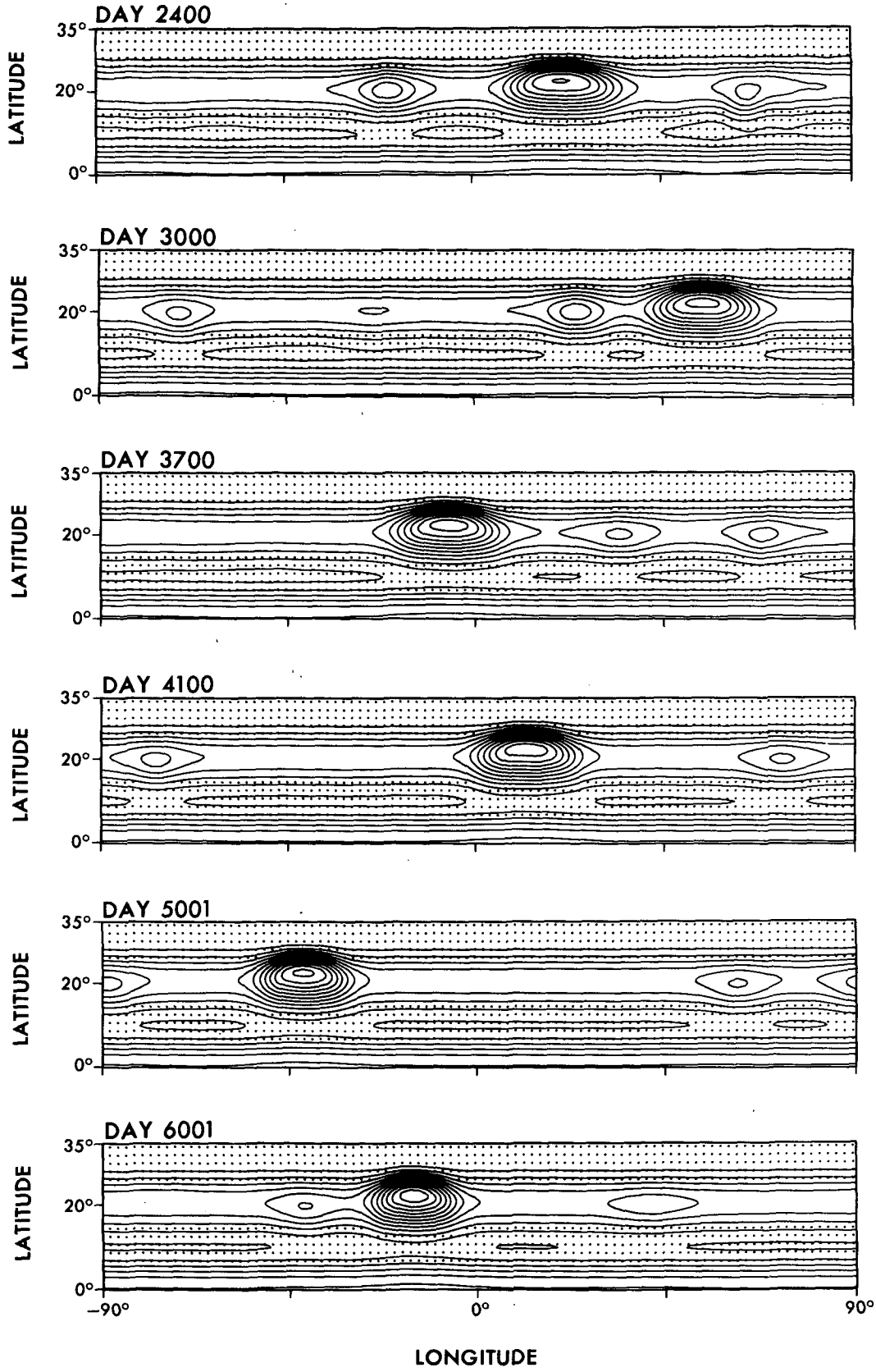

FIG. 24. (*Continued*) Initial state: $(u, v)_0 = U\,\mathrm{sech}^2\{(\lambda - \lambda_0)/\delta\lambda\}\,\mathrm{sech}^2\{(\theta - \theta_0)/\delta\theta\}(\cos k\lambda, -\sin k\lambda)$, with $U = 0.3$ m s^{-1}, $\delta\lambda = 20°$, $\delta\theta = 3°$, $\lambda_0 = 0°$, $\theta_0 = 20°$ and $k = \pi/9$, applied to geostrophic $u_J(\theta)$ jets with $(W_1, E_1, W_2) = (100, -32, 20)$ m s^{-1} and $\theta_{1,2,3,4} = (0°, 10°, 20°, 30°)$.

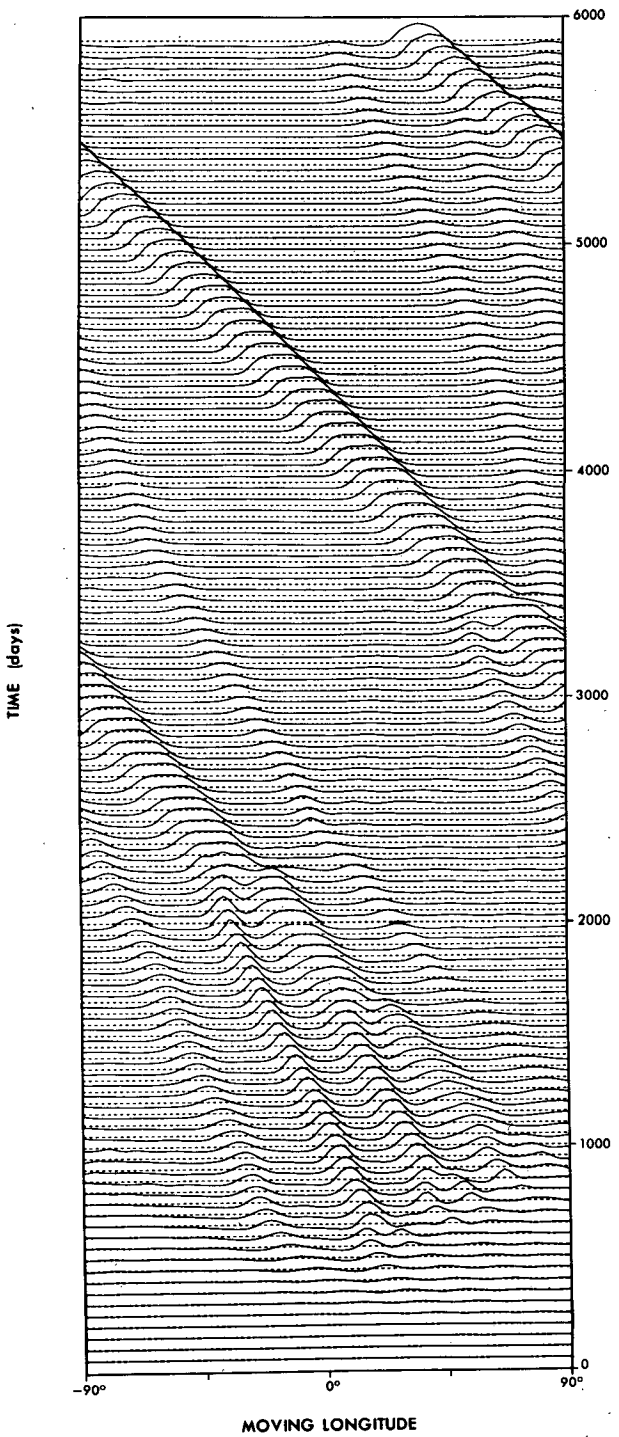

FIG. 25. Time section for the Genesis-1 solution. Height $\eta(\lambda, t)$ at $\theta = 20°$ has axes moving at $c_a = -11.2$ m s^{-1}.

cyclones prevail and by day 500 have broadened, attained a 4-km height, and moved 5° south to the edge of the westerlies. After this buildup, the vortices start to interact and lose their periodicity. Mergers (pairings) at days 640, 680, 720, 770, 780, 830, 860 and 920 reduce the system from 10 to 2 vortices (Fig. 28). Of the two vortices emerging at day 920, the eastern one is 20% stronger and faster and soon catches the other (Fig. 27). The single vortex that results from this final encounter persists and strengthens continuously by absorbing the disturbances created by the forced highs;

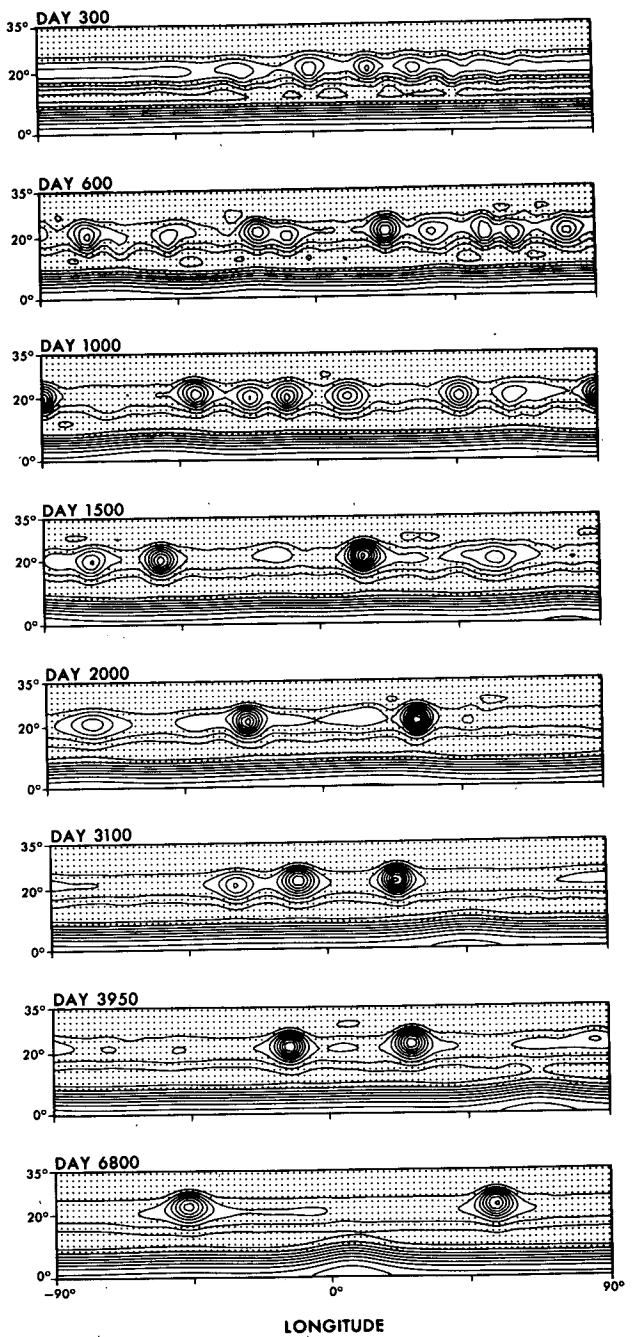

FIG. 26. Low-latitude solution Genesis 2: Generation of two long-lived anticyclones from a wave-packet perturbation of narrow unstable currents. Height η has CI = 1.5 km. Resolution: R2. Initial state: as Fig. 24 but with $(W_1, E_1, W_2) = (100, -30, 14)$ m s^{-1} and $\theta_{1,2,3,4} = (0°, 12°, 20°, 28°)$.

the amplitude grows from 7 km at day 1550 to 11 km at day 3200. In the absence of any dissipative mechanism this vortex will continue to grow.

The various mergers reduce the westerly drift of the anticyclones, but a significant easterly drift arises only with the emergence of the two-vortex state at day 920. The drift rates of the double- and single-vortex states, at -2 m s^{-1} and -5 m s^{-1}, are considerably less easterly than in unforced flows. The drift is made more westerly by the direct interaction between each vortex and the ageostrophic W_2 current rather than by an indirect interaction via the waves, as a selective switching off of the two forcings confirms. In other Genesis cases, the vortex drift is not modified because the currents are in geostrophic balance. The vortex can even be made to move in the opposite direction (eastward) by increasing the W_2 forcing: e.g., boosting the jet to 50 m s^{-1} at day 3500 changes the drift from -5 m s^{-1} to $+5$ m s^{-1} (Fig. 29). The present drift rates of the GRS (-3.5 m s^{-1}) and the Large Ovals ($+4$ m s^{-1}) encompass a similar range.

9. Conclusions

Our numerical single-layer model, based on the Arakawa-Lamb conserving scheme and using a very weak, biharmonic friction, allows vortices to exist virtually indefinitely when they are physically capable of doing so. We find that stable anticyclones can exist at all latitudes but under constraints that vary from midlatitudes to low latitudes to the equator. They occur in a variety of sizes, most much larger than L_R, and in a variety of balances involving the propagation, steepening, dispersion, advection and twisting processes.

Of the various processes involved in vortex dynamics, the vorticity advection proves to be the most flexible and the most effective in stabilizing the flow, which it does by trying to restore radial symmetry. Twisting is the most disruptive process for a large vortex and it limits the development of radially symmetric states. The Rossby-KdV elements, however, still control the storm's size, strength, and speed. Previous studies underestimate the role of twisting and advection in vortex dynamics and display a historical bias towards KdV dynamics.

In midlatitudes, the largest Rossby vortices are dominated by a planetary-geostrophic (PG_2) balance in which the tendency to break by steepening is countered by vorticity advection. The midsize vortices are dominated by an intermediate-geostrophic (IG) balance in which steepening and advection match dispersion and twisting. The small vortices, unlike the larger vortices, migrate in latitude and allow a stable cyclonic form; they are dominated by a quasi-geostrophic (QG) balance between vorticity advection and dispersion. Very small vortices have a modified QG balance between dispersion and the advections of vorticity and kinetic energy.

At the equator, anticyclones are stable only when they have the Hermite latitudinal form and the KdV longitudinal form defined by Boyd (1980). These restrictions exclude twisting and limit interactions. The $n = 1$ mode is the most stable and exists for a wide range of amplitudes. The $n = 3, 5, \cdots$ modes are limited to weaker amplitudes for stability; stronger amplitudes lead to the ejection of lower-n modes. Soliton interactions occur between anticyclones with the same meridional order (n); quasi-soliton interactions occur between those with closely related meridional orders, e.g., $n = 3$ and 5. Equatorial vortices exist in a balance between the dispersion and the KdV-nonlinear term provided by the latitudinally-integrated vorticity advection and height-steepening. Equatorial vortices can exchange energy with and be induced by low-latitude vortices when an equatorial westerly jet exists to (almost) stabilize the latter.

In low latitudes, vortex evolution is dominated by a long-wave meridional dispersion that cannot be countered by advection but can be reduced by zonal flows. Currents stabilize low-latitude vortices by setting up a wave guide in which the equatorial westerly excludes all but the largest modes and the easterly eliminates the twisting and mode generation.

Strong easterly jets become unstable and energize periodic waves that evolve into solitary waves when their wavelength is much larger than the Rossby radius. Wave-packet perturbations develop into unequal anticyclones that merge into a single vortex when the anticyclonic zone is broad, and into double or triple vortex states when the zone is narrow. Stochastically energized small vortices also merge, by pairing, into a single, strong, stable vortex that continues to grow in a turbulent environment. Ageostrophic (pseudo-baroclinic) westerly jets make vortex drift less easterly, or even westerly.

The SL Rossby vortices provide a simple prototype for Jupiter's Great Red Spot. They imply that the GRS was generated by the barotropic instability of the easterly jet or by the baroclinic instability of the westerly jet and is maintained by a continuing instability and by eddy absorption. The GRS could exist freely if dissipation were negligible. Evolution (interaction history) mainly determines the number of vortices in a zone, but the uniqueness of the GRS is also due to its large size and extensive longitudinal influence, features allowed by the broad anticyclonic zone. The Large Ovals are smaller because they lie in a narrower zone and are multiple because they have a limited longitudinal influence. The stochastically forced solution suggests that the GRS should be stable in a turbulent environment and could absorb some of its energy. The Ovals and Rossby vortices have similar developmental timescales: about 10 years. The hemispheric asymmetry and strong eastward propagation of Jupiter's Plumes (at $\theta = 8°$N) eliminate any connection with the equatorial Rossby

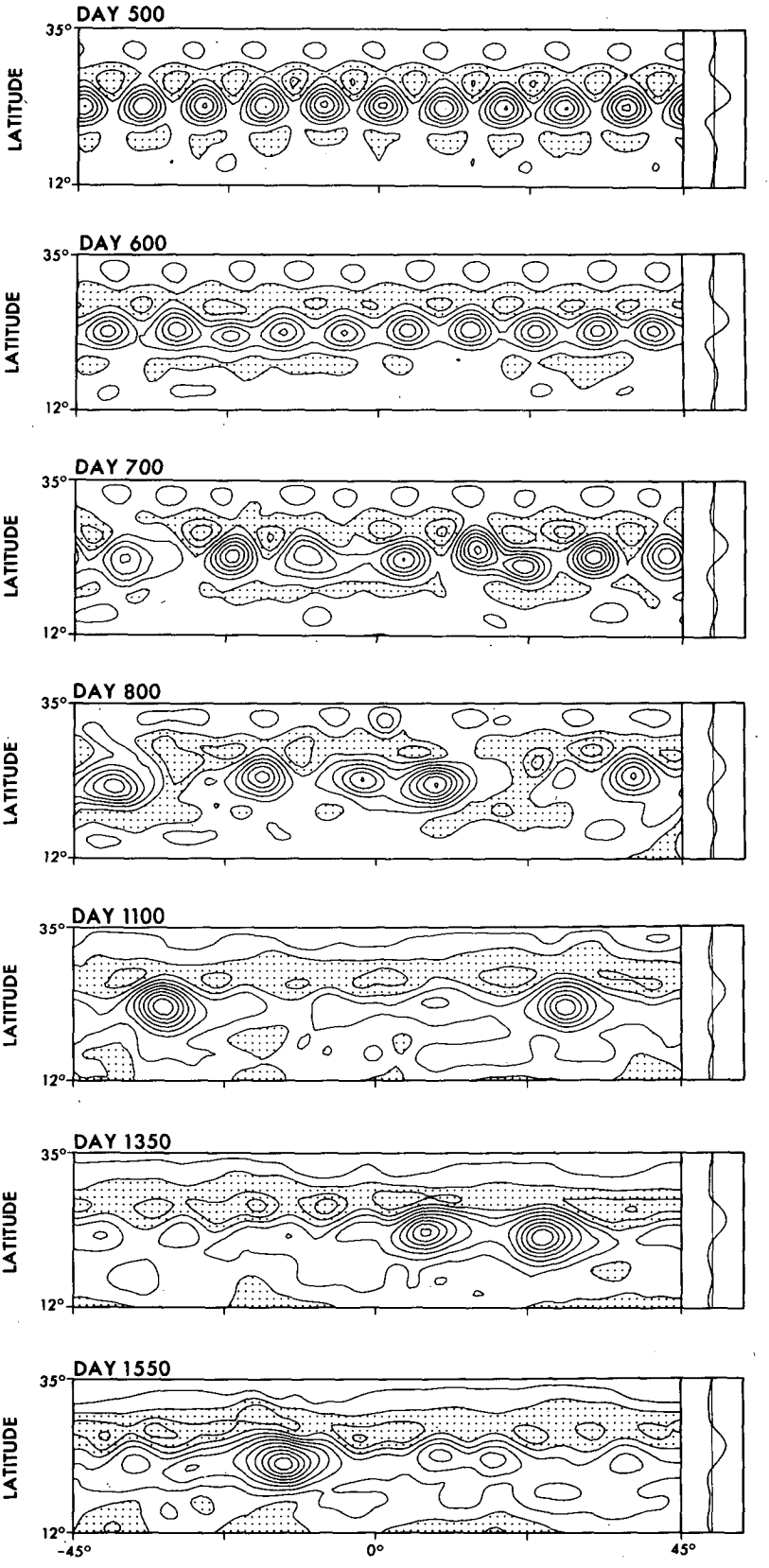

FIG. 27. Low-latitude solution Genesis 3: Generation of a single long-lived anticyclone from stochastically-forced eddies. Height η has CI = 1 km and shading below 2 km. Zonal flow profile has 50 m s^{-1} scale. Resolution: R3. Prediction domain: $\lambda = \pm 45°$, $\theta = 0°$–$35°$.

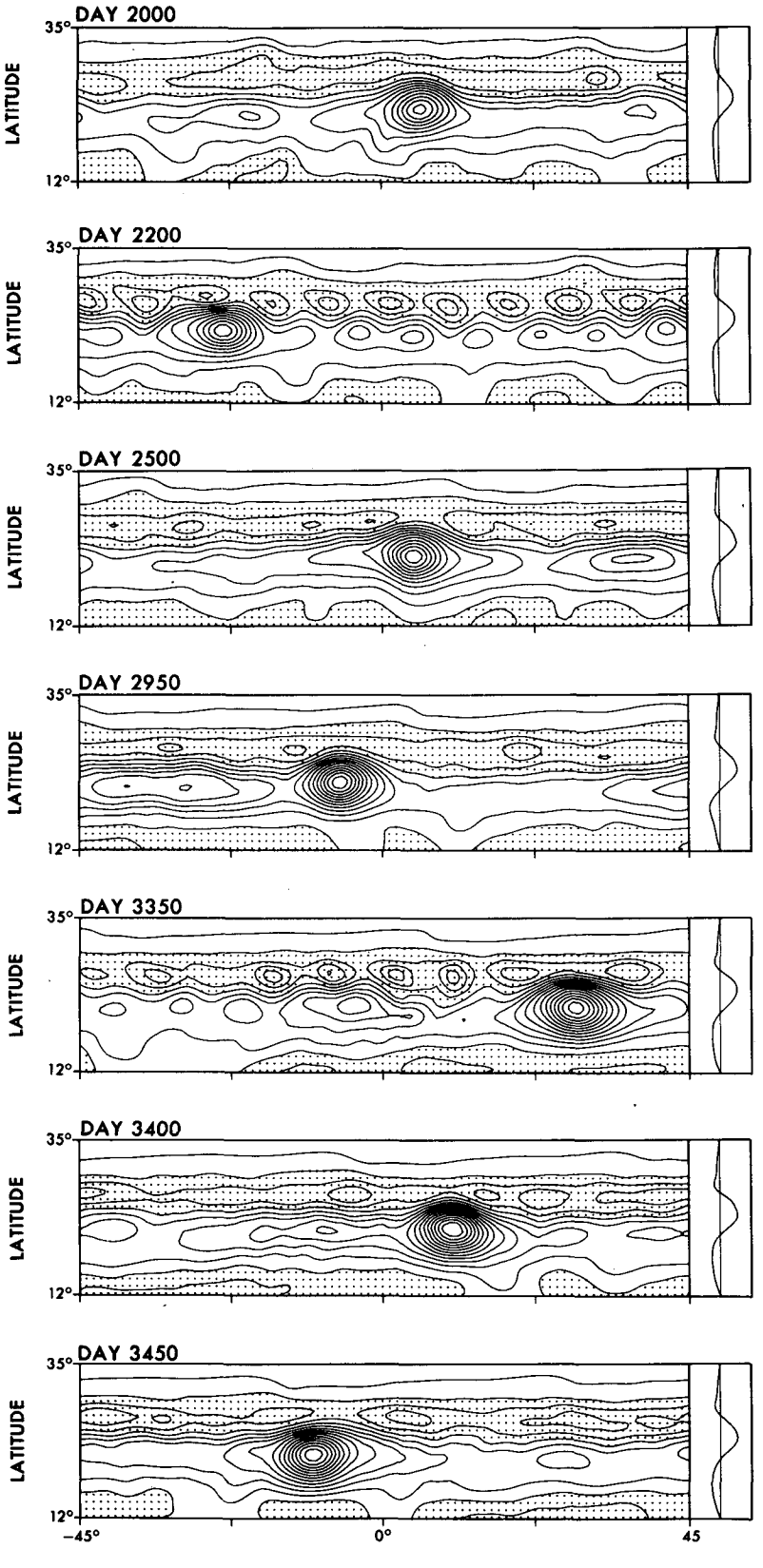

FIG. 27. (*Continued*) Initial state: equatorial jet with $W_1 = 100$ m s^{-1} and $\theta_{1,2} = (0°, 10°)$. Forcing: (i) for W_2 jet, $F\tau^{-1} = 0.5F_a \sin\{\pi(\theta - \theta_0)/\delta\theta\}$ in v_t equation; (ii) for eddies, $F\tau^{-1} = F_a \cos[2\pi(\lambda - \lambda_0)/\delta\lambda] \sin\{\pi(\theta - \theta_0)/\delta\theta\}$ in h_t equation; where $F_a = 0.2$ cm s^{-1}, $\tau = 10^5$ s, $\delta\lambda = 9°$, $\delta\theta = 10°$, $\theta_0 = 25°$, λ_0 random in time, and $20° \leqslant \theta \leqslant 30°$.

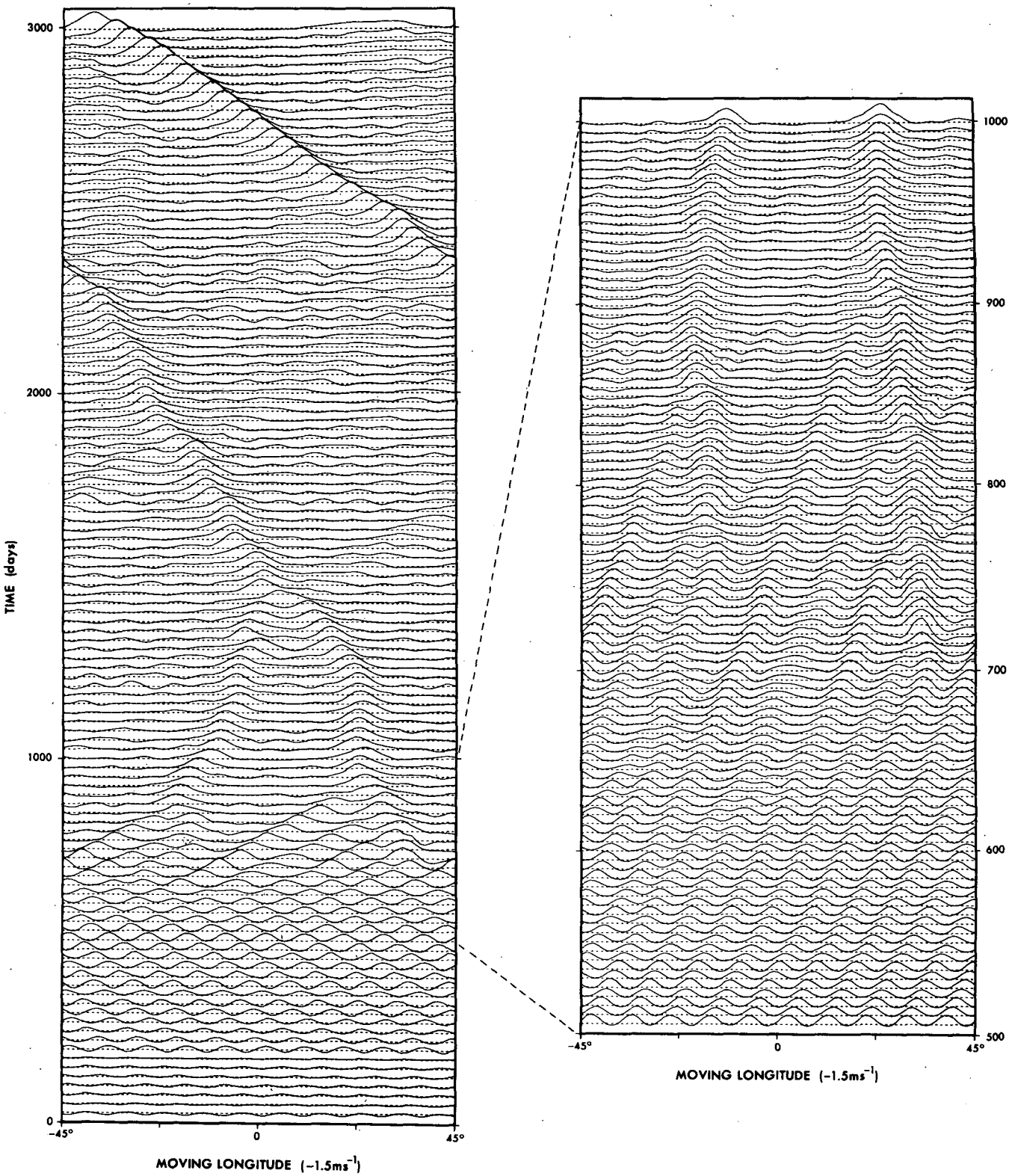

FIG. 28. Time sections for the Genesis-3 solution. Height $\eta(\lambda, t)$ at $\theta = 20°$ has axes moving at $c_a = -1.5$ m s^{-1}. Data shifted eastward by about 30°. Closeup illustrates initial mergers.

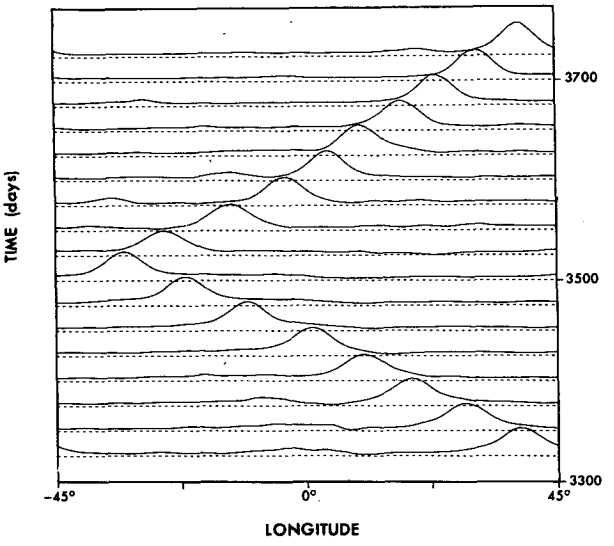

FIG. 29. Time section for an extension to the Genesis-3 solution: Development of westerly propagation. Height $\eta(\lambda, t)$ at $\theta_0 = 20°$ has stationary axes. Direct forcing of the W_2 jet is increased four-fold at day 3500.

vortex, but their size is consistent with the view that only the longest modes can propagate in this region.

Changes in the GRS size could be due to either a change in the zone width or a change in the energy level. Although the GRS has only half the length it had a century ago, it could be stronger. The GRS drift rate, represented by $c = u^F - (\beta - u_{yy})L_R{}^2(1 + H_0/3H)$ in the SL system, could vary because of changes in either the vortex amplitude (H_0), the forced (baroclinic) component of the westerly jet (u^F), the static stability defining the mean thickness (H) and the Rossby radius (L_R), or the lateral shear (u_{yy}).

Four stages of GRS behavior have been observed: 1) in the high-drift Cassini phase, the vortex was small (14 000 km) and moved rapidly westward at -10 m s^{-1} in 1665 and at -8 m s^{-1} in 1670; 2) in the low-drift phase (1840–1880), the vortex was large (40 000 km) and propagated uniformly at -1.5 m s^{-1}; 3) in the transitional phase (1880–1940), the vortex shrank to a medium size (26 000 km) and its drift rate ranged from -5 m s^{-1} to $+1$ m s^{-1} while averaging -2.7 m s^{-1}; and 4) in the medium-drift modern era (1940–1986), the vortex propagated almost uniformly at -3.5 m s^{-1} and shrank slightly to 25 000 km.

Our solutions cover all of the observed variations in GRS size and drift and imply that: 1) the Cassini vortex was the GRS in an early stage of development, with its drift rate close to c_β because u^F was weak or lacked influence on a small storm; 2) the low-drift phase occurred because larger vortices are influenced more by u^F; 3) during the transitional phase, the changes in the drift rate and u^F were correlated, going from -2.7 and 50 m s^{-1} for the 1900–1945 period to -3.5 and 35 m s^{-1} for the 1945–1965 period; and 4) the increased easterly drift of the modern era is due to the increased amplitude of the vortex. These variations in the drift rate suggest that GRS behavior is modulated by a global energy cycle with a period of O(50 years)—changes are imminent—and by a W_2 westerly jet whose 40 m s^{-1} flow has a 10 m s^{-1} baroclinic component.

The Large Ovals (at $\theta = -33°$) arose at the same time (1939) as the GRS increased its easterly drift to -3.5 m s^{-1}. This coincidence suggests that both phenomena were energized by the same energy release at the end of the transitional era. The Large Ovals' reduction in drift and size, from $+7.5$ m s^{-1} and 70 000 km in 1941 to $+4$ m s^{-1} and 12 000 km in 1986, is consistent with an increase in amplitude. A stronger u^F influence (baroclinicity) could account for the drift being more westerly than in the GRS case. The Small Ovals (at $\theta = -41°$) have a size (6000 km) that may be close to the minimum for vortex stability; the critical size lies between 5000 km and 10 000 km for SL vortices at $\theta = 45°$.

The GRS is a low-latitude vortex and its stability depends on the existence of the equatorial westerly and low-latitude easterly jets. The storm may lie in a transitional zone between the geostrophic regime that produces the alternating jets in midlatitudes and the quasi-Hadley regime that produces the westerly jet near the equator. Geostrophic potential-vorticity analyses suggest that both the GRS and the Large Ovals exist in an IG dynamical balance.

Acknowledgments. We are most grateful to C. Raphael, P. Tunison, J. Varanyak and J. Connor for drafting and photography, and to J. Kennedy and W. Marshall for typing.

APPENDIX

Numerical GPV Equation

To balance accurately, the discrete geostrophic potential vorticity (GPV) equation must be carefully defined using the following Sadourny (1975) formulation of the basic equations:

$$\delta_t \bar{u}^t - m^{-1}\bar{q}^y\bar{v}_*^{xy} = -m^{-1}\delta_x(gh + K) + D(u), \quad \text{(A1)}$$

$$\delta_t \bar{v}^t + \bar{q}^x\bar{u}_*^{xy} = -\delta_y(gh + K) + D(v), \quad \text{(A2)}$$

$$\delta_t \bar{h}^t + m^{-1}(\delta_x u_* + \delta_y v_*) = D(h), \quad \text{(A3)}$$

where

$$q = f_* + \zeta_* = \frac{m}{\overline{mh}^{xy}}(f + \zeta),$$

$$\zeta = m^{-1}[\delta_x v - \delta_y(mu)], \quad \text{(A4)}$$

and

$$u_* = u\bar{h}^x, \quad v_* = mv\bar{h}^y. \quad \text{(A5)}$$

To evaluate the terms in the exact GPV equation (6), the geostrophic momenta must be extracted from (A1) and (A2) in the form

$$\overline{u_*^g}^{xy} = -\frac{g}{\overline{f}_*^x}\delta_y h, \quad \overline{v_*^g}^{xy} = \frac{g}{\overline{f}_*^y}\delta_x h, \tag{A6}$$

where f_* is the Coriolis term weighted by h^{-1} and m factors. [The Arakawa-Lamb (1981) scheme does not allow such an exact extraction.] The (A6) expressions give u_*^g at the v gridpoint and v_*^g at the u gridpoint. Ageostrophic momenta are defined at the same gridpoints using the expressions

$$\overline{u_*^a}^{xy} = \bar{u}_*^{xy} - \overline{u_*^g}^{xy}, \quad \overline{v_*^a}^{xy} = \bar{v}_*^{xy} - \overline{v_*^g}^{xy}. \tag{A7}$$

The terms of the GPV equation are then evaluated at ζ gridpoints using the averaged height equation

$$\delta_t \bar{h}^{txy} + m^{-1}[\delta_x \overline{u_*^g}^{xy} + \delta_y \overline{v_*^g}^{xy}] + m^{-1}[\delta_x \overline{u_*^a}^{xy} + \delta_y \overline{v_*^a}^{xy}] = D(\bar{h}^{xy}). \tag{A8}$$

Although the geostrophic divergence simplifies in the continuum [see (7)] the discrete form

$$\nabla\cdot(h\mathbf{v}^g) = -gm^{-1}\left[\delta_x\left\{\frac{\delta_y h}{\overline{f}_*^x}\right\} - \delta_y\left\{\frac{\delta_x h}{\overline{f}_*^y}\right\}\right], \tag{A9}$$

does not. The steepening–twisting is extracted from (A9) by subtracting the uniform translation term $c_\beta{}^0 m^{-1}\delta_x \bar{h}^{xy}$.

To examine the four components of $\nabla\cdot(h\mathbf{v}^a)$ in (A8), the ageostrophic velocity balances are written from (A1) and (A2) as

$$m^{-1}\bar{f}_*^y \overline{v_*^a}^{xy} = \delta_t \bar{u}^t - m^{-1}\bar{\zeta}_*^y \bar{v}_*^{xy} + m^{-1}\delta_x K - D(u), \tag{A10}$$

$$\bar{f}_*^x \overline{u_*^a}^{xy} = -\delta_t \bar{v}^t - \bar{\zeta}_*^x \bar{u}_*^{xy} - \delta_y K + D(v). \tag{A11}$$

The processes can then be evaluated at the ζ gridpoints from the following expressions.

(i) Dispersion:

$$\nabla\cdot\left(\mathbf{k}\times\frac{h}{f}\mathbf{v}_t\right) = m^{-1}\left[-\delta_x\left\{\frac{\delta_t \bar{v}^t}{\overline{f}_*^x}\right\} + \delta_y\left\{\frac{m\delta_t \bar{u}^t}{\overline{f}_*^y}\right\}\right], \tag{A12}$$

(ii) Vorticity advection:

$$-\nabla\cdot\left(\frac{\zeta h\mathbf{v}}{f}\right) = -m^{-1}\left[\delta_x\left\{\frac{\bar{\zeta}_*^x}{\overline{f}_*^x}\bar{u}_*^{xy}\right\} + \delta_y\left\{\frac{\bar{\zeta}_*^y}{\overline{f}_*^y}\bar{v}_*^{xy}\right\}\right], \tag{A13}$$

(iii) Kinetic energy advection:

$$\nabla\cdot\left(\mathbf{k}\times\frac{h}{f}\nabla K\right) = m^{-1}\left[-\delta_x\left\{\frac{\delta_y K}{\overline{f}_*^x}\right\} + \delta_y\left\{\frac{\delta_x K}{\overline{f}_*^y}\right\}\right], \tag{A14}$$

(iv) Vorticity diffusion:

$$-\nabla\cdot\left(\mathbf{k}\times\frac{h}{f}D(\mathbf{v})\right) = -m^{-1}\left[\delta_x\left\{\frac{D(v)}{\overline{f}_*^x}\right\} - \delta_y\left\{\frac{mD(u)}{\overline{f}_*^y}\right\}\right]. \tag{A15}$$

Although $\mathbf{v}$ must be replaced by $\mathbf{v}^g$ to interpret (A12)–(A15) in terms of the GPV processes of (9), the approximation is not needed in the numerical evaluation. In the analysis figures, however, the advections are labeled with their simpler Jacobian forms. Calculations show that the formulation gives an accurate balance if the vorticity diffusion is included and if the resolution is high.

REFERENCES

Anderson, D. L. T., and P. D. Killworth, 1979: Nonlinear propagation of long Rossby waves. *Deep-Sea Res.*, **26,** 1033–1049.

Antipov, S. V., M. V. Nezlin, E. N. Snezhkin and A. S. Trubnikov, 1981: Rossby solitons. *JETP Lett.*, **33,** 351–355.

——, ——, —— and ——, 1986: Rossby autosoliton and stationary model of the Jovian Great Red Spot. *Nature,* **323,** 238–240.

Arakawa, A., and V. R. Lamb, 1981: A potential enstrophy and energy conserving scheme for the shallow water equations. *Mon. Wea. Rev.*, **109,** 18–36.

Benjamin, T. B., J. L. Bona and J. J. Mahony, 1972: Model equations for long waves in nonlinear dispersive systems. *Phil. Trans. Roy. Soc. London,* **A272,** 47–78.

Bolin, B., 1956: An improved barotropic model and some aspects of using the balance equation for three-dimensional flow. *Tellus,* **8,** 61–75.

Boyd, J. P., 1980: Equatorial solitary waves. Part 1: Rossby solitons. *J. Phys. Oceanogr.*, **10,** 1699–1717.

——, 1983: Equatorial solitary waves. Part 2: Envelope solitons. *J. Phys. Oceanogr.*, **13,** 428–449.

——, 1984: Equatorial solitary waves. Part 3: Westward-traveling modons. *J. Phys. Oceanogr.*, **15,** 46–54.

Charney, J. G., 1973: Planetary fluid dynamics. *Dynamic Meteorology.* P. Morel, Ed., Reidel, 97–351.

——, and G. R. Flierl, 1981: Oceanic analogues of large-scale atmospheric motions. *Evolution of Physical Oceanography.* B. A. Warren and C. Wunsch, Eds., The MIT Press, 504–548.

Clarke, R. A., 1971: Solitary and cnoidal planetary waves. *Geophys. Fluid Dyn.*, **2,** 343–354.

Cushman-Roisin, B., 1986: Linear stability of large, elliptical warm-core rings. *J. Phys. Oceanogr.*, **16,** 1158–1164.

Dritschel, D. G., 1986: The nonlinear evolution of rotating configurations of uniform vorticity. *J. Fluid Mech.*, **172,** 157–182.

Flierl, G. R., 1979: Baroclinic solitary waves with radial symmetry. *Dyn. Atmos. Oceans,* **3,** 15–38.

——, 1984: Rossby wave radiation from a strongly nonlinear warm eddy. *J. Phys. Oceanogr.*, **14,** 47–58.

Gill, A. E., 1982: *Atmosphere-Ocean Dynamics.* Academic Press, 662 pp.

Golitsyn, G. S., 1970: A similarity approach to the general circulation of planetary atmospheres. *Icarus,* **13,** 1–24.

——, and L. A. Dikii, 1966: Oscillations of planetary atmospheres as a function of the rotational speed of the planet. *Izv. Atmos. Oceanic Phys.*, **2,** 137–142.

Ingersoll, A. P., 1973: Jupiter's Great Red Spot: A free atmospheric vortex? *Science,* **182,** 1346–1348.

——, and P. G. Cuong, 1981: Numerical model of long-lived Jovian vortices. *J. Atmos. Sci.*, **38,** 2067–2076.

Killworth, P. D., 1979: On the propagation of stable baroclinic Rossby waves through a mean shear flow. *Deep-Sea Res.*, **26A,** 997–1031.

Lindzen, R. S., 1967: Planetary waves on beta-planes. *Mon. Wea. Rev.*, **95,** 441–451.

——, and K. K. Tung, 1978: Wave overreflection and shear instability. *J. Atmos. Sci.*, **35,** 1626–1632.

Long, R. R., 1964: Solitary waves in the westerlies. *J. Atmos. Sci.*, **21,** 197–200.

Malanotte-Rizzoli, P., 1982: Planetary solitary waves in geophysical flows. *Adv. Geophys.*, **24,** 147–224.

Maxworthy, T., and L. G. Redekopp, 1976: A solitary wave theory of the Great Red Spot and other observed features of the Jovian atmosphere. *Icarus,* **29,** 261–271.

McWilliams, J. C., and G. R. Flierl, 1979: On the evolution of isolated, nonlinear vortices. *J. Phys. Oceanogr.,* **9,** 1155–1182.

Petviashvili, V. I., 1980: Red Spot of Jupiter and drift solitons in a plasma. *JETP Lett.,* **32,** 619–622.

——, 1983: Solitary vortices subject to zonal flow in a rotating atmosphere. *Sov. Astron. Lett.,* **9,** 137–138.

——, and V. N. Yankov, 1982: Two-layer vortices in a rotating stratified fluid. *Doklady,* **267,** 825–828.

Redekopp, L. G., 1977: On the theory of solitary Rossby waves. *J. Fluid Mech.,* **82,** 725–745.

——, and P. D. Weidman, 1978: Solitary Rossby waves in zonal shear flows and their interactions. *J. Atmos. Sci.,* **35,** 790–804.

Ripa, P., 1983: General stability conditions for zonal flows in a one-layer model on the β-plane or the sphere. *J. Fluid Mech.,* **126,** 463–489.

——, and S. G. Marinone, 1983: The effect of zonal currents on equatorial waves. *Hydrodynamics of the Equatorial Ocean.* J. C. J. Nihoul, Ed., Elsevier, 291–317.

Romanova, N. N., and V. Y. Tseytlin, 1985: Solitary Rossby waves in a weakly stratified medium. *Atmos. Oceanic Phys.,* **21,** 627–630.

Sadourny, R., 1975: Compressible model flows on a sphere. *J. Atmos. Sci.,* **32,** 2103–2110.

Sagdeev, R. Z., V. D. Shapiro and V. I. Shevchenko, 1981: The Great Red Spot as a synoptic vortex in the Jovian atmosphere. *Sov. Astron. Lett.,* **7,** 279–281.

Williams, G. P., 1978: Planetary circulations 1: Barotropic representation of Jovian and terrestrial turbulence. *J. Atmos. Sci.,* **35,** 1399–1426.

——, 1979: Planetary circulations: 2. The Jovian quasi-geostrophic regime. *J. Atmos. Sci.,* **36,** 932–968.

——, 1985a: Geostrophic regimes on a sphere and beta plane. *J. Atmos. Sci.,* **42,** 1237–1243.

——, 1985b: Jovian and comparative atmospheric modeling. *Adv. Geophys.,* **28A,** 381–429.

——, and T. Yamagata, 1984: Geostrophic regimes, intermediate solitary vortices and Jovian eddies. *J. Atmos. Sci.,* **41,** 453–478.

Yamagata, T., 1982: On nonlinear planetary waves: A class of solutions missed by the traditional quasi-geostrophic approximation. *J. Oceanogr. Soc. Japan,* **38,** 236–244.

Yeh, T.-C., 1949: On energy dispersion in the atmosphere. *J. Meteor.,* **6,** 1–16.